The daughter-parent plot: a tool for analyzing thermochronological data

Birk Härtel and Eva Enkelmann

Department of Earth, Energy and Environment, University of Calgary, Calgary, T2L 1N4, Canada

Correspondence to: Birk Härtel (birk.haertel@ucalgary.ca)

Abstract. Data plots of daughter against parent concentration (D-P plots) are a potential tool for analyzing low-temperature thermochronology, similar to isochron plots in radioisotopic geochronology. Their purposes are to visualize the main term of the radiometric age equation – the daughter-parent ratio – and to inspect the daughter-parent relationship for anomalies indicating influences of geological processes or analytical bias. The main advantages of D-P plots over other data-analysis tools are: (1) their ability to detect systematic offsets in D and P concentrations, (2) their unambiguous representation of radiation damage dependent daughter retention, and (3) the possibility to analyze potential age outliers. ~~Plots of daughter against parent concentration (D-P plots) are widely used as isotope ratio plots in geochronology. Their main purposes are: (1) to visualize the main ingredient of the radiometric age equation – the daughter-parent ratio – and (2) to inspect the daughter-parent relationship for anomalous behaviour indicating influences of geological processes or analytical bias.~~ Despite the~~ir~~se benefits, they are currently not used for analyzing low-temperature thermochronology ~~data~~ data, e.g. from fission track, (U-Th)/He or zircon Raman dating. ~~This contribution aims at putting D-P plots on the map as a data analysis tool.~~ We present a simple, decision-tree-based classification for daughter-parent relationships based on the D-P plot that places a dataset into one of seven classes: linear relationship with zero intercept, cluster, linear relationship with systematic offset, non-linear relationship, several age populations, scattered data, and inverse relationship. Assigning a class to a dataset enables to choose further data analysis~~ -~~ steps and how to report a sample age, e.g. as pooled, central or isochron age, or a range of ages. This classification scheme aims at facilitating thermochronological data analysis and making decisions more transparent. We demonstrate the proposed procedure by analyzing published datasets from a variety of geological settings and thermochronometers and introduce Incaplot, a graphical-user-interface software, that we developed to facilitate D-P plotting of thermochronology data. ~~the right algorithm to calculate a sample age, e.g. as pooled, central or isochron age, or a range of ages. We discuss how to deal with small sample sizes and the possibility of comparing data across samples and chronometers. Our simple classification scheme uses the information in the D-P for facilitating thermochronological data analysis and making it more consistent and traceable.~~

1 Introduction

The isochron plot is a universal tool for analyzing geochronological results, e.g., U-Pb, Ar-Ar or Rb-Sr data (e.g., Nicolaysen, 1961). ~~Plots of radiogenic daughter (D) vs. radioactive parent (P) concentrations (D-P plots, isochron plots) or their isotopic ratios are a standard tool for analyzing geochronological data (e.g., Kulp et al., 1952; Nicolaysen, 1961), such as U-Pb, Ar-Ar or Rb-Sr data.~~ The main reason for ~~their~~ its use is that the ratio of the isotope ratios (e.g., $^{87}Sr/^{86}Sr$ vs. $^{87}Rb/^{86}Sr$) on the plot's axes is the essential term of the radiometric age equation. The slope and intercept of an isochron fitted to a dataset convey information about the age and initial isotopic composition of a sample. ~~the daughter-parent ratio is the main ingredient of determining a radiometric age.~~ Furthermore, the isochron~~D-P~~ plot ~~also~~ enables us to visualize anomalous features in the data, such as outliers ~~or,~~ or excess of radiogenic daughters~~., parent loss, etc.~~

The isochron plot's equivalent for low-temperature thermochronology is the radiogenic daughter (D) vs. radioactive parent (P) plot (D-P plot), which several authors suggest for analyzing fission-track (FT), (U-Th)/He (He), and zircon Raman (ZR) data (e.g., Fanale and Kulp, 1962; Green, 1981; Wernicke and Lippolt, 1993; Dunkl, 2002; Vermeesch, 2008; He et al.,

2021; Härtel et al., 2022a). This plot allows to: (1) detect systematic offsets in daughter or parent concentration (e.g., Vermeesch, 2008); (2) analyze the influence of radiation-damage on daughter retention while avoiding spurious associations (Härtel et al., 2022a); and (3) evaluate single-grain ages in terms of a two-dimensional distribution (e.g., for detecting outliers), or selecting a sample age (e.g., as a mean, pooled, central, or isochron age). The D-P plot thus occupies the interface between the analytical results and more specific data-analysis tools such as radial, kernel-density-estimate (KDE), or age-grain size plots. It is therefore surprising that the D-P plot is not considered a standard tool for analyzing thermochronological data (e.g., Flowers et al., 2022; Kohn et al., 2024).

~~Surprisingly, D-P plots have no wide application in low-temperature thermochronology, despite several authors suggesting them for the fission-track (FT) and (U-Th)/He (He) dating methods (Green, 1981; Wernicke and Lippolt, 1993; Dunkl, 2002; Vermeesch, 2008). The D-P plot allows a different perspective on thermochronological data than the commonly used age-(e)U, radial or age-grain size plots (Vermeesch, 2008; Flowers et al., 2022; Härtel et al., 2022a). It also helps to identify potentially problematic factors such as 'parentless helium' (Vermeesch, 2008) and provides criteria for selecting an appropriate age to report for a sample, e.g. as a mean, pooled, central, isochron age etc. (Vermeesch, 2008; Härtel et al., 2022a).~~

Our aim is to fill this gap and provide guidance to users of low-temperature thermochronology. We envision the D-P relationship as a tool that helps to decide which data-analysis techniques are applicable or not to a given dataset. ~~This article aims at proposing the D-P plot as a first step for analyzing FT, He or zircon Raman (ZR) data.~~ We first provide theoretical background of the D-P plot, its differences to the classic isochron plot, and give examples of ~~discuss the background of the D-P plot and classify the~~ commonly observed daughter-parent relationships. Then, we present a workflow for analyzing daughter-parent relationships. ~~Based on each of these relationships, we~~, suggest data-analysis tools for each type of relationship and, if applicable, provide calculation algorithms to derive a sample age. We introduce Incaplot, a free graphical-user-interface software dedicated to create D-P plots that allows an easy implementation of our proposed analysis to any FT, He, or ZR data. ~~further steps of data analysis and calculation algorithms for sample ages. We then present a set of example data and finally discuss the use and limitation of D-P plots for small datasets, multiple samples, and detrital thermochronology. Our D-P-based approach to analyze thermochronological data is easily integrated into any FT, He, or ZR analysis and allows thermochronologists to trace their decisions during data analysis.~~

2 Background

2.1 Deriving the D-P plot

Using a plot of daughter (D) against parent (P) concentration rests upon the general age equation:

$$t = \frac{1}{\lambda} \ln\left(1 + c\frac{D}{P}\right) \qquad (1),$$

where t is the age, λ is the decay constant, and c is a constant to balance out the units of D and P. ~~The actual quantities of D and P depend on the dating method. For FT dating, D are the spontaneous-track densities and P are either the induced track densities (i.e. external detector method) or U concentration measured using a LA-ICP-MS. For (U-Th)/He dating, the α-ejection corrected He concentration represent the daughter concentration. However, defining a parent concentration is difficult, because several α-emitting nuclides — ^{238}U, ^{235}U, ^{232}Th (and ^{147}Sm) — have to be considered. One solution is to express the parents as an effective uranium concentration (eU) — the sum of the parent concentrations weighted by their relative He production rate (e.g., Härtel et al., 2023), and thereby reduce the number of parents to one:~~

~~$$eU = 1.05[U] + 0.24[Th] + 0.0012[Sm] \qquad (2).$$~~

~~Appendix A discusses the formulation of eU in Eq. (2) and its differences to others (e.g., Shuster et al., 2006; Cooperdock et al., 2019). For ZR dating, the radiation-damage density represents the daughter concentration and the parent concentration is~~

2.2 ~~**Data patterns for multi-grain samples**~~

It is evident from (1) that the age has a one-to-one relationship with the ratio D/P. Therefore, the position of a data point in a plot of D vs. P indicates the single-grain age by the slope of a tie line connecting it to the origin of the plot . ~~(Fig. 1).~~ The D-P plot is thus the graphical representation of the age equation.
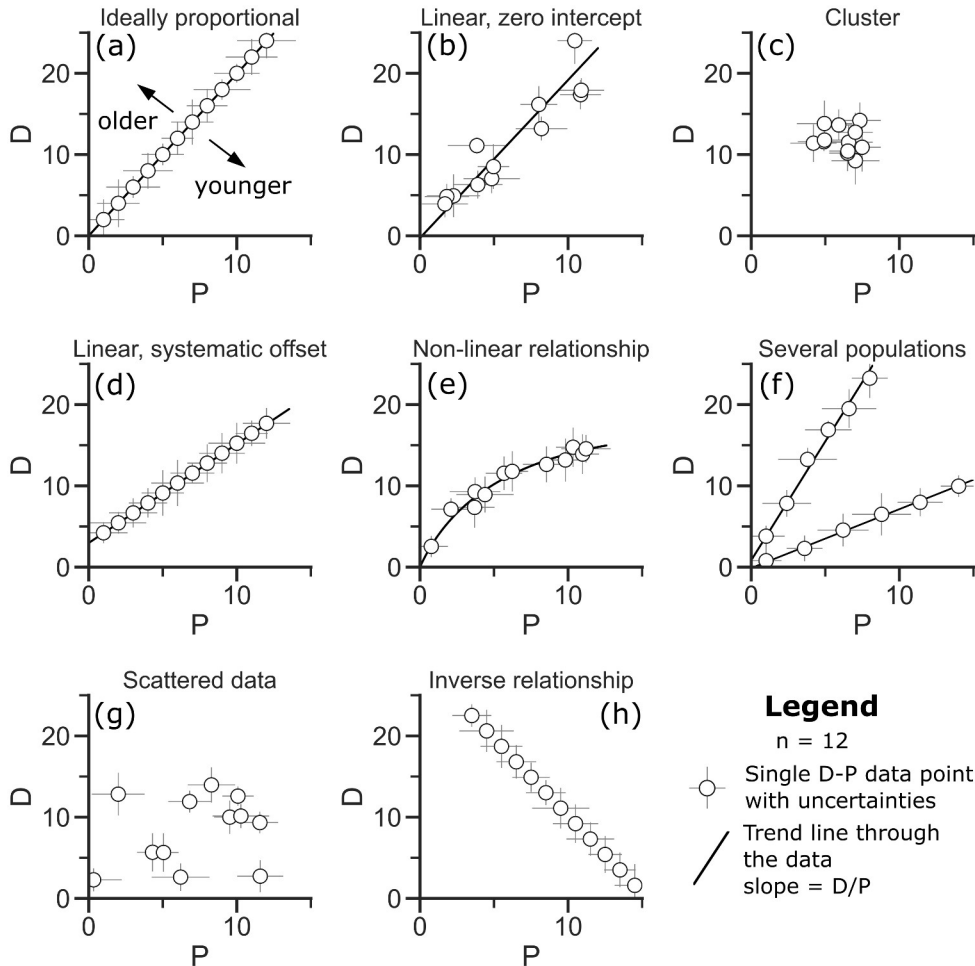
Figure 1. Synthetic data showing different daughter-parent relationships. Sect. 2.2 discusses the possible causes for data falling into each of these classes. Note, that the mean D/P ratio for each panel is 2.

The relationship of the D-P plot to the age equation is the same as that of the classic isochron plot, but there are two significant differences: (1) the isochron plot represents parent and daughter concentrations as isotope ratios with a non-radiogenic sister isotope as the common denominator. This creates error correlation between the two axes of the plot, which is not present in the D-P plot as it relies on independently measured daughters and parents. (2) The isochron plot assumes the initial presence of the radiogenic daughter isotope, which makes isochron fitting indispensable for age calculation. In contrast, for the D-P plot no initial daughters are assumed, enabling the analyst to examine the D-P relationship for patterns without the need for an isochron. To honour these differences, we prefer the generic term *D-P plot* over *isochron plot* for this type of diagram for FT, He, and ZR data.

The actual quantities of D and P depend on the dating method. For FT dating, the daughters are the number or areal density of spontaneous tracks and the parents are either that of induced tracks (external detector method) or U concentration (LA-ICP-MS-based dating). The daughters for (U-Th)/He and zircon Raman dating are the α-ejection corrected He concentration and the radiation-damage density, respectively. However, defining a parent concentration for these methods is difficult,

because several α-emitting nuclides – [238]U, [235]U, [232]Th (and [147]Sm) – have to be considered. One solution is to express the parents as an effective uranium concentration (eU) – the sum of the parent concentrations weighted by their relative α-production rate and thereby reduce the number of parents to one. Appendix A discusses the calculation of eU as a parent concentration in (U-Th)/He and zircon Raman dating and the differences between existing eU equations (e.g., Cooperdock et al., 2019; Härtel et al., 2023). Appendix B provides additional discussion on the choice of daughter and parent concentration units for different dating methods.

2.2 Data patterns for multi-grain samples

In practice, the analyst acquires multiple single-grain data to extract information about a sample's thermal history~~determine a sample age~~. The number of these single-grain analyses varies between methods and analytical protocol – from about 20-30 grains per sample for FT and ZR dating to only 3~~– to~~ 5 grains per sample for whole-grain He dating. The D-P plot allows us to analyze such multi-grain samples. In the ideal case data pairs from same-age grains plot on a line through the origin (Fig. 1a). However, real data deviate from this ideal trend. Figure 1b-h show synthetic data as examples for these deviations, which can be summarized into seven classes. Their patterns may point to geological processes~~, analytical biases, or simply statistical outliers that need to be addressed during data analysis~~ that influence rock cooling and heating. Summarizing thermochronological ages by a ~~a sample~~ mean age without examining the daughter-parent relationship thus does injustice to the data and may neglect important information. To illustrate that, the mean D/P ratio for all the data in the panels of Fig. 1 is 2 and hence the mean age is the same – however, their appearance varies drastically. ~~In addition, deviations from the ideal proportional relationship (Fig. 1a) create spurious correlations in age-(e)U plots (Chayes, 1949; Härtel et al., 2022a).~~ In the following, we give a short overview of the shown classes of typical deviations from the ideal proportional D-P relationship. Fig. 1b presents a positive linear D-P relationship with a zero intercept, including random variation about the trend. This is similar to the proportional case ~~the ideal situation expected~~ with uncertainty on the D and P measurements. Additional variation may be the consequence of varying grain sizes or inaccurate α-ejection correction for He dating, inter-grain chemical differences for FT or ZR dating, and parent-concentration-zoning for all three methods. The D-P plot in Figure 2a shows an example of a linear relationship with a zero intercept for laser-ablation apatite He data from Fish Canyon Tuff (Pickering et al., 2020).
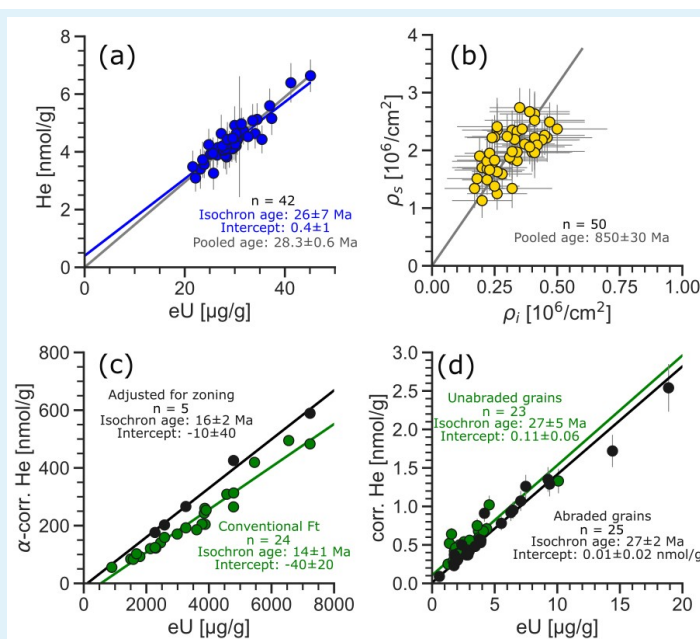
Fig. 2. Examples of linear and clustered D-P relationships. (a) D-P plot of laser-ablation apatite He data

125

Fig. 1c shows clustering of D-P data. This pattern is typical for data from samples with limited inter-grain differences in parent (and daughter) concentrations, and usually their uncertainty intervals overlap strongly. In this case, the positive relationship between daughters and parents may be obscured by the ~~data's~~ uncertainty. Figure 2b shows a D-P plot with clustered apatite FT data from sample FC-1 from the Duluth Complex, Minnesota (Härtel et al., 2022a). Despite relatively
130 large differences in track density, the uncertainties in D and P of most grains overlap.

In Fig. 1d, the data form a linear trend as in Figs. 1a and b, but are offset from the origin. In He dating, such an offset may result from (1) 'parentless helium' implanted by inclusions (Vermeesch et al., 2007), ~~or~~ eU-bearing ~~neighbors~~ grain-boundary or neighboring phases (e.g., Murray et al., 2014) or (2) a consistent style of zoning across grains affecting α-ejection correction (e.g., Orme et al., 2015). In FT dating, it may also be due to a bias towards higher or lower track counts
135 (see Green, 1981). In ZR dating, systematic offsets may result from damage-calibration issues, asymmetric Raman bands, or composition-related Raman-band broadening (Kempe et al., 2018; Troch et al., 2018; Härtel et al., ~~2021,~~ 2022b). Note that an over- or underestimation of P causes an apparent offset of opposite sign in D. Figure 2c is a D-P plot showing an example of negative offset in whole-grain zircon He data from a set of four closely spaced samples of Miocene leucogranite from the Greater Himalaya sequence (Orme et al., 2015). The single-grain ages range from 9.9–14.7 Ma (weighted means: 10–12
140 Ma), whereas Orme et al. (2015) expected an age range of 14–17 Ma due to host-rock stratigraphy and other thermochronological data. They explained this by the zircon grains consistently showing compositional zoning with low-eU cores and high-eU rims: this causes more He to be lost by α-ejection than accounted for by conventional Ft-correction (e.g., Hourigan et al., 2005) and leads to the negative offset. They tested this assumption by adjusting Ft of some grains using zoning information from laser-ablation depth drilling (black circles in Fig. 2c). The ages range from 14.8 to 17.0 Ma
145 (weighted mean: 15.6±0.2 Ma). In the D-P plot, these data points fall above the main trend and show insignificant offset from the origin. The isochron ages for both, unadjusted (14±1 Ma) and adjusted data (16±2 Ma) overlap with each other and fall into the expected age range.

Figure 2d shows a D-P plot of multi-grain-aliquot apatite He data from a volcano-sedimentary succession from DSDP Leg 43 (Spiegel et al., 2009) with a positive offset. Their aliquot ages range from 25 to 80 Ma, with half the aliquots giving ages
150 above 30 Ma. Spiegel et al. (2009) expected the ages to fall in a range of 26.5–29.5 Ma based on stratigraphic and micro-paleontological evidence. These authors argued that the apatite grains experienced He implantation from neighboring high-eU phases. To test this assumption they carried out additional analyses on abraded grains from the same sample to eliminate the implantation effect (black circles in Figure 2d). Data from these aliquots span an age range of 22–42 Ma and the regression line fitted to them does not show a significant offset. This confirms that the surplus helium causing the positive
155 offset was in the outer parts of the apatite grains. Using the D-P plot we show that the isochron ages for unabraded (27±5 Ma) and abraded grains (27±2 Ma) are identical within uncertainties and are both within the expected age range.

Figure 1e showcases a non-linear D-P relationship. This may be due to the daughter retention depending on the degree of lattice damage from α-decay of U, Th and their daughters. The production of radiation-damage is roughly proportional to the parent (eU) concentration. Its effect on daughter retention causes D and P to form either a concave (Fig. 1e, damage-
160 enhanced loss) or a convex (damage-enhanced retention) relationship (Härtel et al., 2022a). Figure 3a shows an example for a non-linear D-P relationship due to radiation-damage-enhanced helium loss in zircon He dating. The shown dataset from the

Minnesota River Valley (Miltich, 2005) consists of several samples assumed to have shared the same thermal history since ~1.8 Ga based on earlier thermochronological data (see references in Miltich, 2005). The He concentration increases approximately linearly with eU increasing up to 500 µg/g and falls at higher eU concentrations in response to radiation damage facilitating He loss from the zircon crystals. Guenthner et al. (2013) suggested a thermal history for these samples based on the zircon radiation-damage accumulation and annealing model (ZRDAAM, black line), consistent with the D-P relationship.

The D-P plot in Figure 3b gives an example for damage-enhanced loss in titanite He data from several Archean samples from the Kaapvaal craton (Baughman et al., 2017) assumed to share the same thermal history since ~1.2 Ga based on thermochronological constraints. Like Figure 3a, He and eU show a linear relationship for eU concentrations ≤80 µg/g and turn into a falling trend at higher eU, levelling off at eU >200 µg/g. In this case, not only the D-P plot, but also radiation-damage measurements by Raman spectroscopy on selected titanite grains support the influence of radiation damage on the titanite He age.

The data in Fig. 1f form two different trends, indicating different age components within the sample. This relationship may occur if a sample contains groups of grains with a high contrast in kinetic properties. Figure 3c shows a D-P plot for an example of different age populations found in apatite FT data for a fully reset sedimentary sample from the Mackenzie Basin, Northwest Territory (Issler et al., 2005). It displays two roughly linear trends in the data corresponding to two different ages. Color-coding the data by chlorine shows a slight compositional difference between the two age populations, suggesting a chemical influence on FT annealing properties (e.g., Barbarand et al., 2003).

; an example for this are the high- and low-Cl apatite grains in the FT data of Stockli et al. (2001).
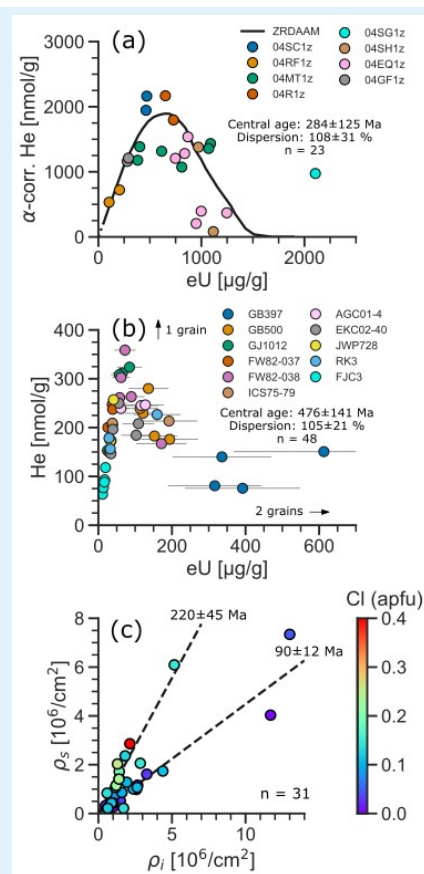
Fig. 3. Examples of non-linear and several-population D-P relationships. (a) D-P plot of whole-grain zircon He data showing a non-linear, concave relationship (samples from Miltich, 2005). The line represents the predicted D-P trend of a zircon radiation-damage and annealing model (ZRDAAM) from Guenthner et al. (2013). The dotted line segment on the left connects the ZRDAAM estimate with the origin. (b) D-P plot of whole-grain titanite He data showing a non-linear,

In Fig. 1g, random scatter obscures the relationship of D and P. Such a pattern can arise due to multiple reasons, e.g., heterogeneous daughter retention within the , e.g. a broad range of grain sizes or chemical compositions. Other reasons for scattered data might be the occurrence of micro-cracks, deformation, or parent zoning. In addition, scatter may arise from analytical factors, such as variably biased α-ejection correction, counting bias, or a combination of these factors. sample due to grain size, chemical composition, micro-cracks, deformation, or parent zoning, analytical reasons, such as inaccurate α-ejection correction or counting bias, or a combination of factors.
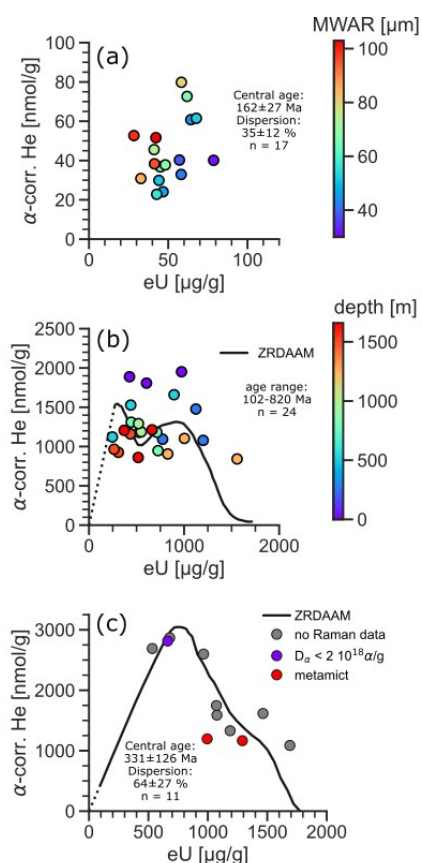
Figure 4. Examples of scattered and inverse D-P relationships. (a) D-P plot of multi-grain-aliquot apatite He data showing a scattered relationship (data from Reiners and Farley, 2001). The data are color-coded by grain size expressed as mass-weighted average radius (MWAR). (b) D-P plot of whole-grain zircon He data showing a scattered relationship (data from Guenthner et al., 2017). The line represents the predicted D-P trend from ZRDAAM, and the dotted line segment on the left connects to the origin. (c) D-P plot of whole-grain zircon He data showing an inverse relationship (sample A10-42 from Ault et al., 2018 and Armstrong et al., 2024). Color-coding indicates radiation-damage measurements using a Raman microprobe. The line represents the predicted D-P trend from ZRDAAM, and the dotted line segment on the left connects to the origin. All uncertainties are 2s.

An example of a scattered D-P plot can be found in the multi-grain-aliquot apatite He data from the Bighorn Mountains, Wyoming (Reiners and Farley, 2001). The data show no relationship between He and eU (Fig. 4a). However, color-coding

the different aliquots by the mass-weighted average radius (MWAR) reveals an age (i.e., D/P ratio) increase with increasing grain size. This indicates a continuous age distribution due to different sensitivity of differently sized grains to volume diffusion of helium. Figure 4b shows another example of a scattered D-P relationship in whole-grain zircon He data. It uses a set of borehole samples from the Fennoscandian Shield and color-codes the data by sampling depth (Guenthner et al., 2017). The black line represents the ZRDAAM from the original publication. However, neither the depth of each sample – and thus their current temperature – nor the radiation-damage model explain the scatter in the data. In this case, an unknown factor underlies the age variation.

Figure 1h shows an inverse relationship between daughters and parents. This pattern may occur due to (1) a small sample size causing a spurious relationship (Ketcham et al., 2018), (2) bias from over- or under-correcting the He concentration for α-ejection, or (3) the data representing a falling segment of a non-linear trend caused by radiation damage. Figure 4c provides an example for a negative D-P trend from whole-grain zircon He data. Ault et al. (2018) interpreted the age variation in this dataset as due to radiation-damage enhanced He loss, as the ZRDAAM (black line) in Figure 4c shows. Armstrong et al. (2024) provided Raman data on selected grains, showing that some of the zircon grains with eU ≥ 1000 µg/g were metamict, explaining their low He concentration compared to the lower-eU grains. (1) the data representing a falling segment of a non-linear trend, (2) a small sample size causing a spurious relationship (Ketcham et al., 2018) or (3) bias from over- or under-correcting the He concentration for α-ejection.

Each of the shown relationships requires different considerations for data analysis. This includes the questions if reporting a single sample age is appropriate, and if yes, which type of sample age to report. In addition, the D-P plot allows to identify the relative position of outliers with respect to the rest of the data, showing if its main deviation occurs in D or P. It also helps to decide if a radiation-damage model is necessary to understand the geological history of the sample, and which other data-analysis tools may provide further insights. Thus, the D-P plot contains essential information for translating data into time-temperature information.

Our ability to evaluate the D-P relationship for a sample clearly depends on the number of data. While this is not a concern for FT and ZR dating (n>10), it is a limiting factor for conventional whole-grain He dating (n<10). However, the recent development of laser ablation based He dating will increase the number of grains analyzed per sample and recognizing D-P relationships (e.g., Tripathy-Lang et al., 2013; Pickering et al., 2020). We discuss the limitations of D-P plots for small samples in sect. 4.1.

2.3 Unique benefits of D-P plots

Figures 1–4 show the variation of thermochronological data in terms of D-P patterns. Each of these relationships requires different considerations for data analysis. This includes the questions if reporting a single sample age is appropriate, and if yes, which type of sample age to report. Some of the factors causing age variation can be traced by commonly used data-analysis tools such radial plots, KDE, or age-grainsize plots, but there are unique benefits to analyzing data in the D-P plot.

First, the D-P plot is the only thermochronological data plot that enables us to *detect systematic offset* in daughter or parent concentrations (Figs. 1d, 2c, 2d). Systematically offset data pose a serious problem to many standard data analysis tools and should therefore be treated with caution: (1) single-grain ages calculated from offset data are biased towards higher or lower ages depending on the sign of the offset. This bias propagates into calculated central tendencies (Härtel et al., 2022a) and into plots displaying the age as a variable, such as radial, KDE, age-grainsize, and age-(e)U plots. Figure 5a shows a radial plot for the systematically offset zircon He data from Figure 2c. Both, the single-grain ages (9.9–14.7 Ma) and the central age (12.0 ± 0.7 Ma) are substantially younger than the age range of 14–17 Ma, which Orme et al. (2015) expected from stratigraphic and thermochronological constraints. However, the isochron age (14±1 Ma for conventionally analyzed grains, Figure 2c; Appendix C2) fits well with this scenario and agrees with the zoning-corrected ages of 14.8–17 Ma (Orme et al., 2015). The positively offset apatite He data in Figure 2d show a similar good fit of the isochron age (27±5 Ma) with the age

range that Spiegel et al. (2009) expected (26.5–29.5 Ma). In contrast, the central age for these data is biased towards older ages (37±4 Ma for unabraded grains). (2) Offset data appear over-dispersed (and fail the χ^2 test) because the data uncertainties do not explain the spread in age. This further complicates the use of radial plots, as the spread in single-grain ages may give way to a misinterpretation of ages as a mixture of discrete age components (see discussion in Vermeesch, 2019). The data in Figure 5a falling out of the 2 standard-deviation envelope showcase this problem. (3) The over-dispersion by systematic offset hampers inverse thermal-history modeling, as the modeling algorithm will have to reconcile a large spread in ages without the uncertainties accounting for it (e.g., Vermeesch and Tian, 2014). As the offset affects each data point differently, this problem cannot be solved by expanding the uncertainties in D and P (Flowers et al., 2022a). (4) Systematic offset also compromises the Helioplot (Vermeesch, 2010), which determines the age from log-ratios, because it disturbs all ratios derived from the D and P concentrations.

Figure 5. Examples for the unique benefits of the D-P plot. (a) Radial plot of data from Orme et al. (2015) shown in Figure 2c that illustrate the bias caused by systematic offset. The center of the y-axis is the central age calculated from conventionally alpha corrected data. The purple area represents the expected age range from stratigraphic and thermochronological constraints. (b)-(d) Age-eU plots showing negative associations for: (b) data from Miltich (2005) with a non-linear D-P relationship (Figure 3a); (c) data from Guenthner et al. (2017) with a scattered D-P relationship (Figure 4b); (d) data from unabraded grains of Spiegel et al. (2009) with a linear, systematically offset D-P relationship (Figure 2d). All uncertainties are 2s.

Second, the D-P plot provides an unbiased indication if daughter retention in a sample depends on *radiation damage*: the D-P plot shows unambiguous linear relationships for well-documented cases of radiation-damage-dependent daughter retention (e.g., Figs. 3b, 4c; Baughman et al., 2017; Armstrong et al., 2024); in contrast, not all associations observed in the commonly used age-eU plot reflect actual radiation-damage effects (e.g., Carter, 1990; Härtel et al., 2022a): Figures 5b-d show examples of age-eU plots with negative relationships drawn from the datasets shown in Figs. 2–4. However, the D-P plots provide a more nuanced view, showing that only the data in Fig. 5b form a non-linear relationship indicative of radiation-damage effects (Figure 3a); the data in Figs. 5c and 5d also show age-eU associations, while their D-P relationships (Figs. 4b, 2d) do not support an explanation based on radiation damage.

Third, the D-P plot allows to *detect age outliers* in two-dimensional space, not only from single-grain ages (e.g., He et al., 2021). It thus allows to identify the relative position of outliers with respect to the rest of the data, showing if its main deviation occurs in D or P.

3 ~~An analytical~~ Proposed workflow based on D-P plot analysis

As shown above, the D-P plot allows to interpret a range of age patterns in thermochronological data (Figs. 1–4) and has the unique ability to detect a systematic offset or radiation-damage influence, two possible causes for age variation that are not covered well by other data-analysis tools. We therefore suggest the D-P plot as the first step for thermochronological data analysis, before moving on to more specific data-analysis tools such as radial, KDE, or age-grainsize plots, or thermal-history modelling. ~~As Fig. 1 shows, the D-P plot provides a first step into thermochronological data analysis and helps to decide which analytical or geological factors may influence a dataset.~~ We propose a decision-tree approach to classify the daughter-parent relationship (Fig. 6~~2~~). Depending on the class of the relationship, ~~it then suggests~~we then suggest further steps of data analysis. The following sections outline the use of the decision tree to systematically classify the data and find an appropriate description of the contained thermal-history information.

3.1 Preliminary considerations

Before using the classification scheme in Fig. 6~~2~~, it is essential to assure that the analytical procedures and samples meet certain quality criteria established for each method, e.g., that suitable grains were selected for He dating, that data with asymmetric Raman bands were excluded from ZR dating, that track counting was conducted on prismatic grain surfaces, etc. Also, the number of analyses in the dataset is important, as fitting a regression line or splitting a dataset into age populations is not appropriate for small datasets (see sect. 4~~.1~~). Another criterion to be considered is the geological background of the sample. For example, a crystalline bedrock sample with a simple cooling history will likely give a single age, while a metasedimentary rock may show different age populations due to chemical variation between grains, and a volcanic rock recording its eruption is expected to give a near-ideal linear trend.
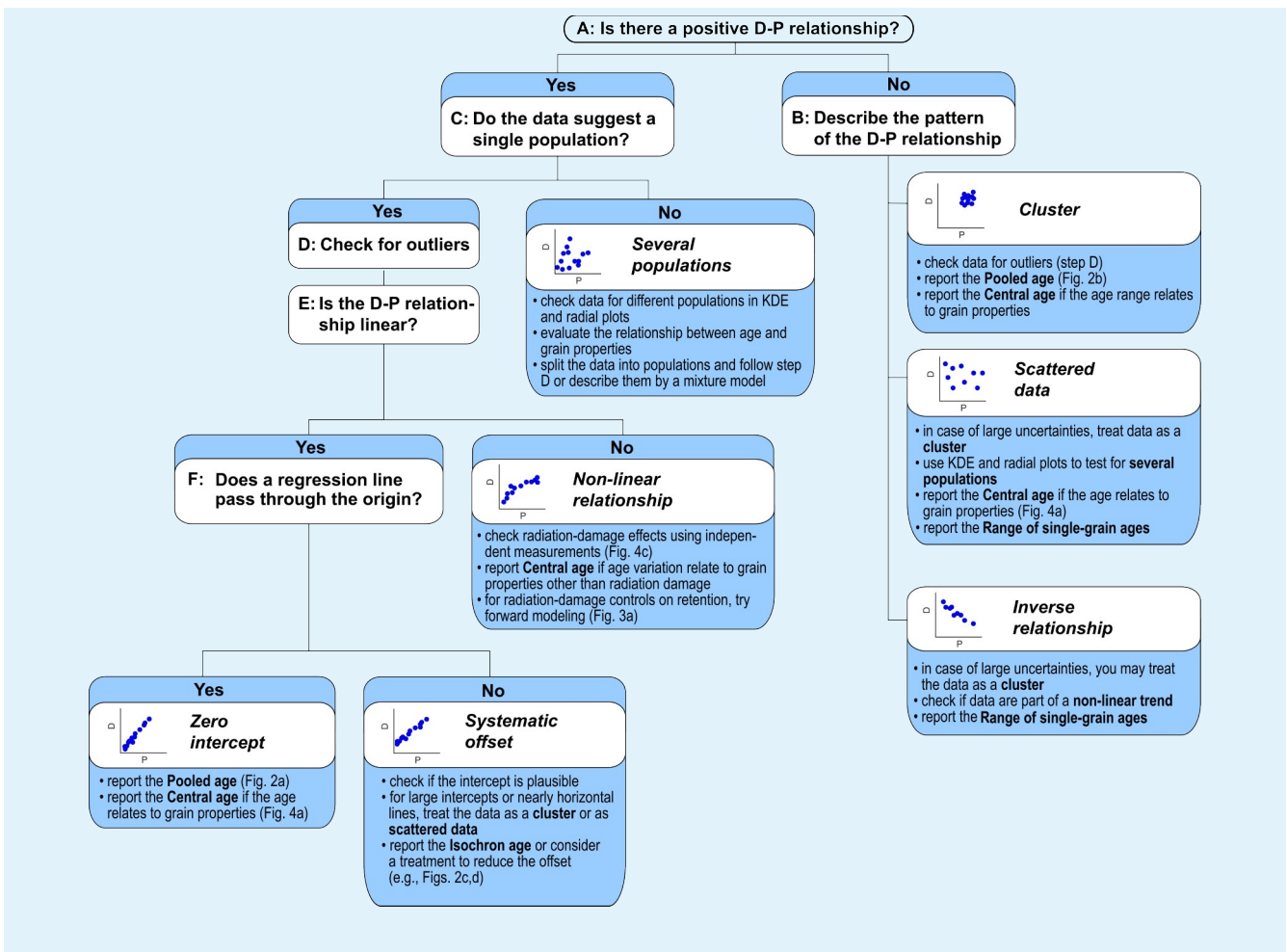
Figure 6. Decision tree for classifying the daughter-parent relationship in a sample (classes named as in Fig. 1). The blue boxes provide suggestions on how to treat data belonging to the respective class.

275 Radiation-damage effects and accompanying non-linear relationships are expected for old rocks with protracted or complex cooling histories, but not for young rocks that did not spend time in the temperature regime of radiation-damage accumulation. The interpretation of a sample that strongly deviates from the geological expectations needs to be carried out with care.

3.2 The classification procedure

280 For analyzing the data, we calculate the daughter and parent concentrations according to the thermochronological method used (see Appendix B) and plot daughters against parents~~them against each other~~. The analysis proceeds by following the decision tree in Fig. 6~~2~~ to classify the daughter-parent relationship.

The first step separates datasets showing a positive D-P relationship from those that do not (A in Fig. 6~~2~~). We expect a
285 positive association between D and P from the radioactive production equation, but this association may be obscured by factors discussed in sect. 2.2. In the case of data, for which the D-P relationship is not clear, it is usually safe to assume that there is no positive relationship – a decision that may be revised in later steps. Data, for which D and P are not positively associated, are then classified as either clustered, scattered or following an inverse relationship (B in Fig. 6~~2; Fig. 1e, g, h~~).
For data with a positive D-P relationship, it is then essential to distinguish datasets containing a single age population from
290 those with several populations (C in Fig. 6~~2~~). As in Figs. 1f and 4a, multiple age populations form linear arrays with different slopes or clusters in the dataset with gaps between them. A ~~kernel-density-estimate (~~KDE~~)~~ plot may reveal the presence of different populations for cases that are not clear-cut.

For single-population data, the next step is filtering the dataset for outliers (D in Fig. 62). Outliers stick out by a difference in single-grain age to the other data beyond their uncertainty. However, this is not sufficient evidence to mark a data pair as anomalous: other factors such as systematic offset may also cause single grains to be significantly older or younger than the others (Fig. 1d). In the D-P plot, outliers show up as removed from the main trend or group of data points. Before, considering such a measurement as anomalous, other properties should be examined, e.g. grain size or mineral chemistry. If anomalous data are excluded from further analysis, this should be reported, e.g. by marking the excluded data point as empty symbol in the D-P plot. For ambiguous cases, it may be advantageous to carry out the further steps with and without the concerned data point. For He dating, Flowers et al. (2022) provide further strategies for treating outliers (their sect. 3.1).
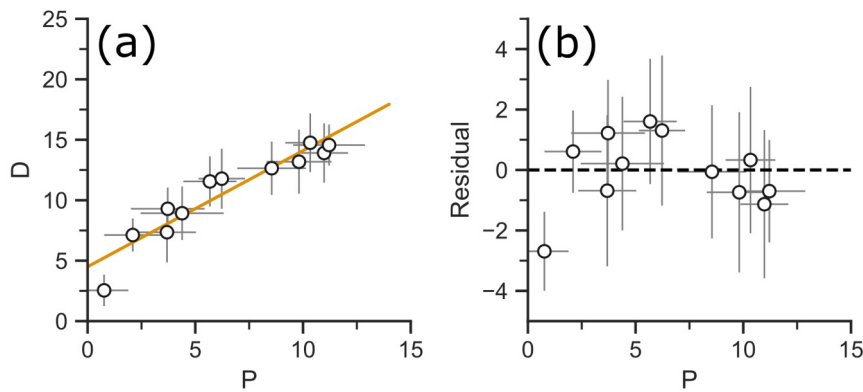
Figure 7. D-P plots for testing for a non-linear relationship. (a) Regression line fit to a synthetic non-linear D-P relationship. (b) Fitting residuals (difference between measured and fitted D).

After examining the outliers, we test the data for a linear D-P association (E in Fig. 62). If it is not clear whether the data show a linear or a non-linear trend from visual inspection alone, this can be verified by fitting a regression line to the data and examining the residuals, i.e. the deviation of the data points from the line. For a linear relationship, the residuals scatter randomly around zero while in the case of a non-linear relationship, there is an association between residual and parent concentration. Fig. 73a shows the linear fit to a synthetic dataset in a D-P plot. Figure 73b plots the fitting residuals against P, revealing a boomerang-shaped trend that points to a non-linear D-P relationship.

If the D-P relationship is linear, it is necessary to test the data for a systematic offset (F in Fig. 62). This is achieved by fitting a regression line to the data and examining its intercept. If the intercept includes zero in its uncertainty envelope, the offset is not significant and the data may be treated as having a zero intercept. If the uncertainty envelope does not include zero, this is a sign for a potential offset. However, this uncertainty on the intercept may be an underestimate if the variation of the data strongly exceeds that expected from the uncertainties (e.g., high MSWD; Wendt and Carl, 1991; see Appendix C). Another simple test for an intercept is the comparison of the isochron age and the pooled age: if the data form a trend through the origin, the two ages should be indistinguishable because the pooled age assumes a zero intercept ~~and should thus be indistinguishable from the isochron age~~ (see sect. 3.43).

3.3 ~~Classes of daughter-parent relationship~~Sample-age calculation

Once arrived at a certain class of D-P relationships, the goal is to assign an age to the sample. This can either be a central tendency, such as a mean or pooled age, or an isochron age for a sample with a single age population, or a number of ages or a range of single-grain age depending on the D-P relationship (Fig. 4, Table 1). If the given ages can be described by a single sample age, the simplest solution is to report a central tendency. Despite its simplicity, the (arithmetic) mean age does

usually not provide a reliable sample age (e.g., Vermeesch, 2008; Härtel et al., 2022a). A more robust alternative is the pooled age, which uses the ratio of the summed D and P concentrations.

If the intra-sample age variation can be related to a certain grain property affecting radiogenic daughter retention, the ages may represent a continuous mixture, with each grain recording a different age due to its individual properties. Figure 3c shows an example with He data varying with respect to grain size. Such a mixture is best described by the central age (e.g. Galbraith, 2005; Vermeesch, 2019).

Datasets, that are systematically offset, require a different approach, that of the isochron age, which rests on the slope of a fitted regression line through the D-P data. If several discrete age components exist in a dataset, these can be separated by mixture modeling (e.g., Galbraith and Laslett, 1993; Vermeesch, 2019), or by treating each age component as a single sample.

If the data cannot be described by a single age or multiple ages, nor by a continuous mixture related to grain properties, it is still possible to report the range of single-grain ages, which does not rely on any model assumptions. Appendix C provides a more detailed discussion about mean and isochron ages, and discrete and continuous age mixtures. The following sections provide suggestions for how to treat data falling into each of the D-P classes of Fig. 2.

3.4 Classes of daughter-parent relationship

3.34.1 Linear relationship with zero intercept

If the daughter-parent relationship is linear and the intercept of its regression line is close to zero (F in Fig. 62), the pooled and the isochron age are similar (Fig. 1b2a). In this case, it is advantageous to report the pooled age, which is more robust and does not require the intercept as additional parameter. As all single-grain ages along the linear trend are roughly the same, the potential bias of the pooled age is negligible (see Appendix C).

If the MSWD or spine factor of the fitted regression line (F in Fig. 62) are outside the upper confidence limit, the data are over-dispersed. This points to two possible scenarios: (1) Analytical dispersion due to the uncertainties not reflecting the actual measurement error. This is especially a problem for He and laser-ablation FT dating (e.g., Fitzgerald et al., 2006; Ketcham et al., 2018; Cogné and Gallagher, 2021). In this case, the uncertainty on the pooled age may be expanded to take into account the variation of the individual analyses (see Eq. (C6) in Appendix C). (2) Geological dispersion due to heterogeneous grain properties affecting daughter retention, such as grain size, composition etc. This can be tested by plotting the age against these properties, or by using them for color-coding the D-P plot (Fig. 3c4a). If the data are dispersed due to a continuous range of grain properties, the central age describes the age distribution best (Appendix C).

3.34.2 Cluster

Clustered data are best summarized by the pooled age (Fig. 1c2b). To make sure that there is no bias towards the oldest or highest-D-P grains, the data should be screened for outliers (D in Fig. 62). If the data are over-dispersed, e.g., failing the χ^2 test (e.g., Galbraith, 2005), the uncertainty of the pooled age may be expanded to reflect the actual inter-grain age variation (see Eq. (C6) in Appendix C) or the data may be treated as scattered. If there exists a relationship between age and grain properties, e.g. by plotting the age against these grain properties or to color-coding the D-P plot (e.g., Fig. 4a3c), the age distribution may be described by a central age.

3.43.3 Linear relationship with systematic offset

Systematically offset data must be treated with caution as such data pose problems for many common data-analysis tools (see sect. 2.3). The only sample age that may appropriately describes systematically offset data is the isochron age determined from the slope of a regression line (see Figs. 2c, d; section 2.3; Appendix C2Appendix C). Another option is to

360 verify the reason of the intercept, such as zoning, 'parentless helium', or a counting bias (section 2.2) and finding a strategy to eliminate it (e.g., Spiegel et al., 2009; Orme et al., 2015). The intercept of the regression line provides a first-order estimate for the amount of offset~~, that may be interpretable in terms of 'parentless helium' or a systematic property of the analyzed grains~~. If the intercept is large, close to the mean daughter concentration, or if the data allow for a horizontal or vertical line fit, they could also be treated as a cluster (sect. 3.~~3~~4.2) or as scattered data (sect. 3.~~3~~4.6). If the data are over-

365 dispersed, e.g., showing an MSWD outside its confidence interval, it is possible to expand the uncertainty on the isochron age by multiplying it with $\sqrt{MSWD}$ (e.g., Ludwig, 2012). For a strong overdispersion (e.g., MSWD > 10), the data ~~may also~~should be treated as scattered (see sect. 3.~~3~~4.6).

~~Systematically offset data pose a serious problem to many standard data analysis tools and should therefore be treated with caution: first, the offset causes spurious age-(e)U association (Härtel et al., 2022a) due to low-parent data points being more~~

370 ~~offset than high-parent ones (compare grey lines in Fig. 1d). Second, offset data will usually appear over-dispersed (and fail the χ^2 test) because the age deviations are usually not explained by the uncertainties. This complicates the use of radial plots, as the spread in single-grain ages may give way to an interpretation of ages as a mixture of discrete age components (see discussion in Vermeesch, 2019). In addition, this will hamper inverse thermal-history modeling, as the modeling algorithm will have to reconcile a large spread in ages without the uncertainties accounting for it (e.g., Vermeesch and Tian, 2014). As~~

375 ~~the offset affects each data point differently, this problem cannot be solved by expanding the uncertainties in D and P (Flowers et al., 2022a). Fourth, the use of log-ratios for data analysis as in the Helioplot (Vermeesch, 2010) is compromised because the offset disturbs all ratios derived from the D and P concentrations.~~

3.~~4~~3.4 Non-linear relationship

A non-linear relationship in the D-P plot points to radiation-damage-dependent daughter retention. This assumption can be

380 tested against independent radiation-damage measurements. Raman and infrared spectroscopy, or X-ray diffraction provide radiation-damage estimates for zircon or titanite (e.g., Nasdala et al., 1995; Deliens et al., 1977; Holland and Gottfried, 1955; Heller et al., 2019), while optical absorption ~~spectroscopy~~ or Raman spectroscopy are potential tools to measure radiation damage in apatite (e.g., Ritter and Märk, 1984; Liu et al., 2008).

Alternatively, a non-linear D-P relationship could result from daughter retention depending on other grain properties and the

385 different grains recording the same thermal history differently. This effect can be examined by plotting the age against these parameters or by color-coding the D-P plot (Fig. 3~~c~~4a). If such a relationship exists, the dataset may be described by a central age (see Appendix C).

If the decision for a non-linear versus a linear relationship with an offset is not clear (E in Fig. 2~~6~~; Fig. 3~~a~~7a, b), the less complex linear model should be preferred over a non-linear model (sect. 3.~~3~~4.3) in the absence of independent radiation-

390 damage measurements.

For a non-linear trend caused by radiation-damage-dependent daughter retention, forward modeling of daughter retention and radiation-damage accumulation and annealing provides further insight s into a sample's~~the~~ thermal history (e.g., Flowers et al., 2009; Willett et al., 2017; Guenthner et al., 2013). In this case, the D-P plot allows to compare the data to the D-P relationship predicted by the model, especially in the low-eU region, where the model prediction connects to the origin

395 (Härtel et al., 2022a). Figures 3a and 4c show thermal-history forward models for zircon He dating plotted as lines in comparison to the measured data.~~model. Figure 5a shows thermal-history forward models of Guenthner et al. (2013) for zircon He dating plotted as lines in comparison to the measured data.~~

3.~~3~~4.5 Several populations

If the D-P plot suggests that several discrete age components are present in the sample, the KDE or radial plot are the

400 standard tools to examine the data. The occurrence of different components should also be tested for consistency, e.g., if a mixture of populations makes sense in the geological context (sect. 3.1) or by color-coding according to a variable that may underlie the different populations (see Fig. 3c). The age distribution can either be described by a ~~mixing~~finite-mixture

model (e.g., Galbraith and Laslett, 1993; Galbraith, 2005; Vermeesch, 2019) or by separating the data into age components to be analyzed individually according to the procedure in Fig. 6~~2~~.

3.~~3~~4.6 Scattered data

Data that vary strongly in age and are scattered in the D-P plot may result from several scenarios: First, they may be a consequence of underestimating the uncertainties with respect to the variation in the single-grain data (e.g., for He dating, Fitzgerald et al., 2006; Brown et al., 2013). Martin et al. (2023) and Zeigler et al. (2023) showed that especially the uncertainty related to α-ejection correction in whole-grain He dating is difficult to estimate, ~~while α-ejection~~while the correction ~~strongly~~ contributes significantly to the age error. Data with limited scatter, for which the uncertainties may be underestimated ~~could~~ may be treated as a cluster (sect. 3.~~3~~4.2). A second explanation for scatter is the occurrence of different age populations, which can be verified in a KDE plot ~~and may be better observed within a larger dataset~~ (sect. 3.~~3~~4.5). Third, the scatter may also be due to each grain having slightly different daughter-retention properties and recording a different age. Plotting the age against these parameters or color-coding the D-P plot (Fig. ~~3c~~4a) allows to assess this relationship; a central age may be used to describe such a continuous mixture (sect. 3.~~3~~4.2; Appendix C).

If the scatter cannot be explained by one of these scenarios (e.g., Fig. 4b), the range of the single--grain ages should be reported (Table 1). Scattered data also pose a serious problem to inverse (t-T) modeling, as the age difference may not allow for a single t-T path to reconcile the spread in ages.

3.~~3~~4.7 Inverse relationship

An inverse daughter-parent relationship runs contrary to the relationship expected from the age equation (Fig. ~~1b~~4c). In general, while such data should be treated with caution, two scenarios can account for this relationship without pointing to an analytical problem.~~, two scenarios can account for this relationship without pointing to a serious problem with the analyses in question.~~ If the dataset is small (e.g., n≤5), a spurious inverse trend could arise randomly (Ketcham et al., 2018) and the dataset should be treated as scattered (sect. 3.~~4~~3.6). However, the interpretation of small datasets should be carried out with caution (see sect. 4.~~1~~). Alternatively, the inverse relationship may represent an inverse segment of a non-linear trend, if radiation damage controls daughter retention ~~is affected by radiation damage~~ (sect. 3.~~4~~3.4; Fig. ~~4c~~5a). If there is no clear explanation for the inverse daughter-parent relationship, it is best to report the range of single-grain ages (~~Table 1;~~ Appendix C).

~~3.4 Examples and reporting format~~

~~The above classification scheme allows for a clear path of decision to each of the D-P classes. Figure 4 shows three examples for daughter-parent plots, each with a different D-P relationship.~~

~~The ZR data in Fig. 4a form a positive, linear relationship between radiation damage density D and eU. We classify the relationship as having a zero intercept, based on the intercept being within uncertainty of the origin (-1±3 10^16 α/g; F in Fig. 2, sect. 3.2). The age to report in this case is the pooled age. Table 1 presents a reporting format for these data.~~

~~The ZHe data in Fig. 4b form a positive, linear relationship between He content and eU. However, there is a positive intercept (50±30 nmol/g) whose uncertainty envelope does not include the origin. We therefore classify the D-P relationship as linear with an offset and report the isochron age. The AHe data in Fig. 4c form a positive relationship, but they also exhibit much more variation than expected from their uncertainties and fitting a regression line to these data is difficult. We therefore classify the data as scattered. The color-coding by grain size shows that the variation in D and P cannot be~~

440 ~~explained as a consequence of grain size on He diffusion kinetics: the smaller grains contain more He compared to the larger grains. We therefore report the range of single-grain ages (179–301 Ma; Table 1).~~

~~Table 1. Example for reporting data-analysis results based on the D-P plots in Fig. 4.~~

~~Sample name~~	~~Dating method~~	~~D-P relationship~~	~~Age reported~~	~~Age (Ma)~~	~~n~~
~~TDR~~	~~ZR~~	~~Linear, zero intercept~~	~~Pooled age~~	~~55 ± 5~~	~~14~~
~~FC1~~	~~ZHe (whole grain, abraded)~~	~~Linear, offset~~	~~Isochron age~~	~~1030 ± 30~~	~~13~~
~~FC1~~	~~AHe (whole grain)~~	~~Scattered~~	~~Single-grain age range~~	~~179-301~~	~~8~~

3.5 D-P plotting in Incaplot

445 This section briefly describes Incaplot (Härtel, 2024), a simple, Python-based graphical-user-interface software dedicated to producing D-P plots. Existing softwares (e.g., Trackkey, Isoplot Excel, IsoplotR) already provide the tools for D-P plotting, but these are often buried between other functions or are available for certain dating methods only. Incaplot is available for free at https://zenodo.org/records/8233941 as a one-file executable for Mac (MacOS 10.15 Catalina and younger) and Windows operation systems (Windows 8 and younger).
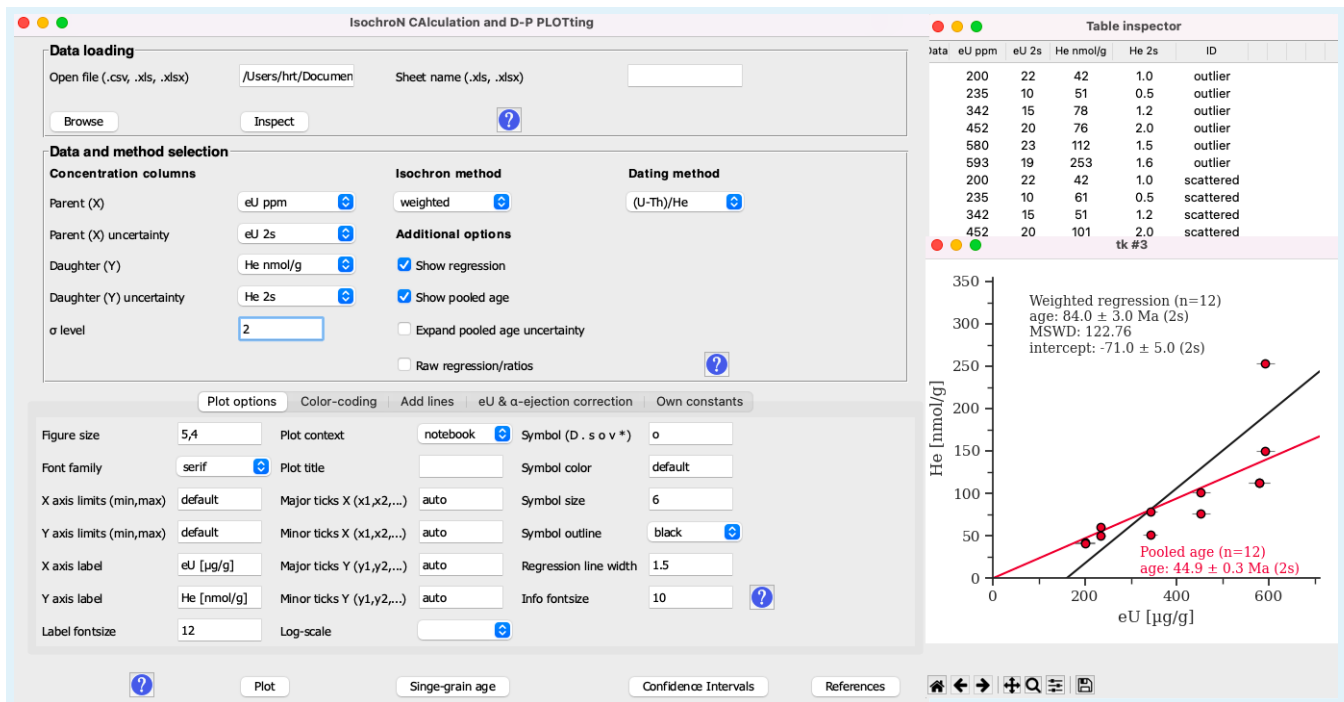
Figure 8. Main window of the Incaplot software (left), the table inspection tool (upper right) and an output D-P plot (lower right).

450 Incaplot allows to create D-P plots and calculating low-temperature themochrometric ages. It also provides a range of visualization and customization options. Figure 8 shows Incaplot's main window (left), its data inspection tool (upper right) and its graphical output (lower right). The main window consists of three frames dedicated to (1) loading data files, (2) the input data and calculation algorithms to be used, and (3) modifying the plots and calculations.

Incaplot requires the input files to be Excel spreadsheet files in .xls, or .xlsx format or comma-separated (.csv) text files. The
455 plotting variables need to be organized as columns with the variable names in the first row. A user manual for the current Incaplot version and an example file displaying the input data format are available in Incaplot's zenodo repository.

Incaplot provides a range of plot-customization options, which include customizing markers, axes and ticks, adding line segments to plots, and color-coding plots by discrete and continuous variables. While Incaplot was set up to handle mainly

He, ZR and FT data, it can also be used for other dating systems or generic scatterplots. The output plots are exportable in different raster (.jpg, .png, .tif) and vector formats (.svg, .pdf, .eps).

Besides D-P plotting, Incaplot contains functions for sample-age calculation as pooled age, isochron fitting with different algorithms (see Appendix C2), calculation of single-grain ages and effective uranium concentrations (see equation (1) and Appendix A).

Table 1. Example for reporting data-analysis results based on the D-P plots in Figs. 2–4.

Sample name(s)	Method	D-P relationship	Age reported	Age (Ma)	n	Comment	Reference	Figure
FCT	AHe (LA)	Linear, zero intercept	Pooled age	28.3±0.6	42	-	Pickering et al., 2020	2a
FC1	AFT (EDM)	Cluster	Pooled age	850±30	50	-	Härtel et al., 2022a	2b
Multiple samples, list in reference	ZHe (WG)	Linear, offset	Isochron age	14±1	24	Conventional Ft correction, Intercept: -40±23	Orme et al., 2015	2c
Multiple samples, 43-2 to 43-8	AHe (MG)	Linear, offset	Isochron age	27±5	23	Unabraded grains, Intercept: 0.11±0.06	Spiegel et al., 2009	2d
Multiple samples, list in Fig. 3a	ZHe (WG)	Non-linear	Central age	284±125	23	Dispersion: 108 ± 31 % Interpretation from radiation-damage model	Miltich, 2005	3a
Multiple samples, list in Fig. 3b	THe (WG)	Non-linear	Central age	476±141	48	Dispersion: 105 ± 21 % Interpretation by radiation-damage-dependent retention	Baughman et al., 2017	3b
I-77	AFT (EDM)	Several populations	Finite mixture ages	220±45 90±12	31	Interpretation by retention depending on chlorine content	Issler et al., 2005	3c
Multiple samples, list in reference	AHe (MG)	Scattered	Central age	162±27	17	Dispersion: 35 ± 12 % Interpretation from grain-size model	Reiners and Farley, 2001	4a
Multiple samples, list in reference	ZHe (WG)	Scattered	Single-grain age range	102-820	24	-	Guenthner et al., 2017	4b
A10-42	AHe (whole grain)	Inverse	Central age	331±126	11	Dispersion: 64 ± 27 % Interpretation from radiation-damage model	Ault et al., 2018; Armstrong et al., 2024	4c

Note: LA – laser-ablation, EDM – external-detector method, WG – whole-grain method, MG – multi-grain aliquot method, AHe – apatite He, AFT – apatite FT, ZHe – zircon He, THe – titanite He. The age uncertainties are 2s.

4 Limits of the D-P plot based data-classification scheme

The data-analysis workflow in Figure 6 provides simple decision paths and criteria for assigning a dataset to a class. This has the advantage to keep the data-analysis process consistent, especially for studies involving many samples. Still, this decision-based approach has some limits that need to be pointed out.

First, not all datasets may be assignable unambiguously to a class. Examples may be cases of moderate variation falling between clustered or scattered data or cases, in which the distinction between linear- and non-linear relationships is not clear (see Fig. 7). While section 3.4 provides suggestions for alternative classifications, this problem highlights the necessity for transparent reporting on the decisions taken by the analyst. We recommend to either show the daughter-parent plot for each sample or at least report the class of the D-P relationship and the type of the reported age to allow retracing the data-analysis process. Table 1 gives an example of a reporting format using the data from Figures 2–4.

4 Further considerations

4.1 Small datasets

Second, our ability to evaluate the D-P relationship for a sample clearly depends on the number of data and the complexity of a sample's geological setting. While the classification with the flowchart in Fig. 2 is useful for larger datasets, it is important to point out its limitations for datasets consisting of few analyses. This concerns especially conventional whole-grain He dating, where sample sizes of ≤5 grains are common. There are several limits a small sample imposes on data analysis: (1) it is not possible to recognize different populations; (2) in terms of sample ages, the small number of grains inhibits the use of isochron or central ages, which would require the fitting of several parameters (age and intercept or dispersion) to a small amount of data. a single outlier may constitute a large proportion of the gathered data; (3) random variation may cause inverse D-P relationships (see Ketcham et al., 2018) or spurious associations between the age and other properties; (4) linear regression becomes useless due to the influence of single data on the regression fit. A classification following Fig. 2 is therefore not possible.

While this hampers a strict classification following Fig. 6, it is still possible to use the D-P plot as a qualitative guide, However, it is still possible to use the D-P plot as a qualitative guide, e.g., to visualize the data in terms of their variation in D and P. It also enables to examine in which D-P direction a potential outlier deviates from the rest of the data. This helps to decide whether a single data point with a different age may bias the pooled age (high D or P) or not (see Appendix C).

In terms of sample ages, the small number of grains inhibits the use of isochron or central ages, which would require the fitting of several parameters (age and intercept or dispersion) to a small amount of data. We therefore suggest using the pooled age or a range of ages.

4.2 Plotting multiple samples

An additional use for the D-P plot is the comparison of thermochronological data from different samples. This mode of analysis usually requires some geographical or geological context and thus belongs to a later step of the data analysis then the single-sample analysis. This data grouping hinges on the condition that the different samples are comparable, e.g., being geographically or geologically related. This strategy is often used for analyzing age-eU associations in apatite, zircon and titanite He dating (e.g., Guenthner et al., 2013, 2017; Baughman et al., 2017; Sturrock et al., 2021). Figure 5a shows grouped zircon He data from the Minnesota River (Miltich, 2005). While the D-P relationships differ strongly between samples, together, they form a non-linear trend that can in part be explained by radiation-damage-dependent He retention (models as lines; Guenthner et al., 2013; sect. 3.3.4).

It is also possible to group data from samples sharing a systematic difference in thermal history, e.g., those collected across a fault, or along an elevation profile or borehole. Comparing them in the D-P plot reveals their age pattern with respect to their position. Figure 5b shows zircon He data of Wolfe and Stockli (2010) from the Kontinentale Tiefbohrung (KTB) drillhole. The D-P plot highlights (1) the systematic difference in age between data from above and below 4 km depth, and (2) the variation in eU at different depths.

For example, this helps to decide if the pooled age is biased towards a single high-D or -P grain (see Appendix C1). In this case, we recommend to check this potential outlier or report the single-grain age range. The number of analyzed grains is not a concern for FT and ZR dating (n>10), but it is a limiting factor for conventional whole-grain He dating (n<10). However, the recent development of laser ablation based He dating will increase the number of grains analyzed per sample and recognizing D-P relationships (e.g., Tripathy-Lang et al., 2013; Pickering et al., 2020). In addition, some cases may allow grouping together data from several small samples. This approach hinges on the condition that the different samples are comparable, e.g., that they share the same thermal history in the partial annealing/retention zone of the used thermochronometer. This strategy is often used for analyzing He data with respect to radiation-damage effects (e.g., Figs. 3a, b; Fig. 4c; Guenthner et al., 2013, 2017; Baughman et al., 2017; Ault et al., 2018; Armstrong et al., 2024).

Last but not least, the D-P enables us to compare the dating results for single samples across methods to: (1) examine age differences, (2) compare the D-P relationship, or (3) unexpected apparent age relationships, e.g. apatite FT-He age inversion (Green et al., 2006; Flowers and Kelley, 2011; Recanati et al., 2017). Figure 5c displays an example of apatite, baddeleyite and zircon He data from the Phalaborwa carbonatite complex, South Africa (Baughman and Flowers, 2018), showing the difference in helium retention and eU content between the three minerals.

4.3 Detrital samples

Third, detrital samples often record a complex mixture of pre- and post-depositional thermal history. They also often contain grains with different chemical composition and size. Detrital samples are therefore not expected to fit into the simple categories of Figure 6. Detrital or sedimentary samples are more complicated than the cases shown here: they usually contain grains with different pre-depositional thermal histories, chemical composition and size. Therefore, eExtracting an age or an

530 interpretation from a single sample or a single thermochronometer is usually not possible (e.g. Carter, 2019). Also, the versatility of detrital samples makes it difficult to trace an observed pattern in the D-P plot to its causes.

Standard procedures for interpreting detrital thermochronological data include identifying peak ages in the single-grain age distribution and putting them into the context of the stratigraphic age, age distributions of source areas, catchment geometry, etc. (e.g., Malusà and Fitzgerald, 2019). While it is possible to evaluate age distributions in the D-P plot (see sect. 3. ~~43~~.5),

535 KDE or radial plots are the more adequate tools for this. Still, the D-P plot may hold additional information that is difficult to access with these plots. First, it may be used on a subset of the data to evaluate the daughter-parent relationship for a given age ~~peak~~ population and possibly detect a non-linear or systematically offset relationship (sect. 3.~~43~~.3, 3.~~43~~.4). However, this can only be done reliably, if enough data (e.g., n ≥10) are available in this grain population. Second, it may help to identify bias in grain selection. One of these is the problem with overlapping, uncountable fission tracks in old or U-rich zircon, that

540 may skew ZFT age populations towards younger ages and thus ~~impact~~ affect the interpretation in terms of source-area exhumation and erosion patterns (e.g., Malusà, 2019).
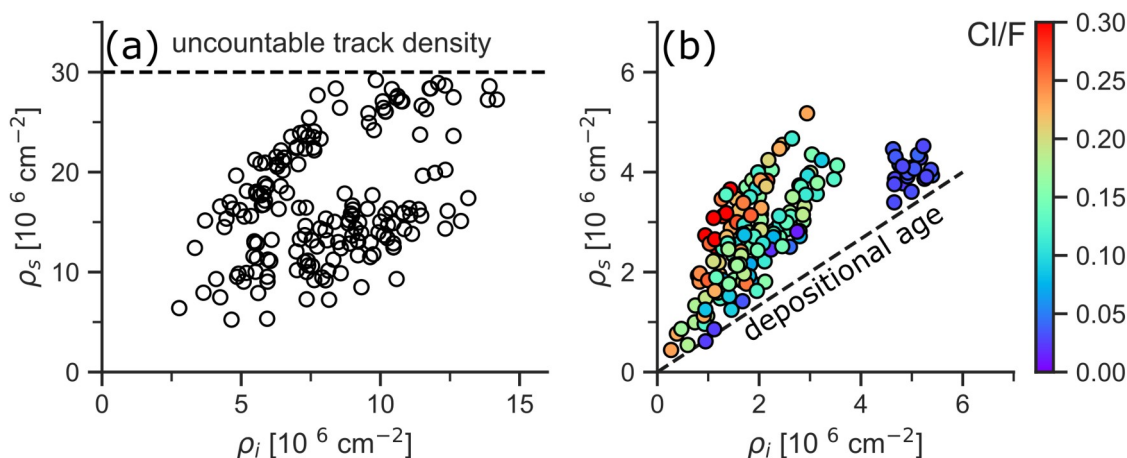
Figure ~~9~~6. Possible applications ~~of~~for D-P plots for detrital thermochronology. (a) D-P plot for a synthetic ZFT dataset with the dashed line marking the density threshold, at which the spontaneous tracks become uncountable. (b) D-P plot for a synthetic AFT dataset color-coded by the Cl/F ratio. The dashed line represents the depositional age.

Figure ~~9~~6a shows the D-P plot for a synthetic ZFT dataset. The dashed line marks the countability limit~~threshold uncountable~~ for the spontaneous tracks. ~~The countability~~This limit cuts off the track-density distribution for an old grain population~~, and thereby~~; it indicates that the sample may contain older or higher-U grains not datable with the ZFT method.

545 A third application is the visualization of different grain populations with respect to age, parent concentration and other grain properties, e.g. grain size or composition to highlight nuances in the composition of different age populations. Figure ~~9~~6b shows the D-P plot for a synthetic AFT dataset with color-coding by the Cl/F ratio and a dashed line representing the

depositional age. In this case, part of the grains in the age group slightly older than the depositional age, stands out due to its high induced-track density (high U content) and its F-dominated halogen composition being dominated by fluorine. So, 550 despite the complexity of detrital samples, there are situations, in which the visualization of the data in a D-P plot can be useful.

5 Conclusions

Plots of daughter vs. parent concentration (D-P plots) represent a graphical solution of the age equation in radiometric dating and are effective to reveal crucial information in low-temperature thermochonrology data. They) are a standard tool in 555 radiometric dating representing a graphical solution of the age equation. D-P plots allow to identify sources of age variation and choose an appropriate algorithm to calculate a sample age. Their unique advantages over other data-analysis tools are their capabilities to detect systematic offsets and radiation-damage effects in the data and the possibility to identify potential outliers with respect to both, daughter and parent concentration rather than the single-grain age only. We show several published datasets exemplifying the range of possible D-P relationships and how they link up to geological factors 560 influencing the age., such as systematic offsets, outliers or the occurrence of several populations. We present a new workflow for using D-P plots in thermochronological data analysis. This approach follows that describes the use of D-P plots for thermochronological data analysis. Our approach follows a step-wise examination of the daughter-parent relationship and assigns one of seven classes to it. This enables us to choose the further steps for data analysis and identify possible factors influencing the age. The classification scheme is an attempt to make data analysis more consistent and transparent.

565 Our classification approach has limitations especially when applied to small or detrital datasets, however, the D-P plot itself can still provide important insights in these cases. We also introduce Incaplot, a free, graphical-user-interface software and invite everyone for creating and customizing D-P plots in a straightforward way.

It also enables thermochronologists to trace back the decisions made during data analysis. While there are limits of D-P plots dealing with small samples, the D-P plot provides many possibilities for comparing data across samples and 570 thermochronometers, for detrital thermochronology and for analyzing data from newly developed dating methods or less routinely used mineral phases (e.g. hematite or baddeleyite He dating, ZR dating).

Appendix A: The effective uranium concentration

The effective uranium concentration (eU) is a summary of the α-producing U, Th, and Sm concentrations, rescaling them to a common decay rate of U:

$$eU = k_U [U] + k_{Th} [Th] + k_{Sm} [Sm] \qquad \text{(A1)},$$

with the terms in the brackets being the concentrations in units of mass, and k_U, k_{Th} and k_{Sm} being coefficients for each concentration. There are currently two definitions of eU that result in slightly different coefficients. Shuster et al. (2006) and Cooperdock et al. (2019) recalculate the actinide concentrations to a concentration of total U, whereas Härtel et al. (2021) recalculate them to the decay rate of ^{238}U only. The latter approach enables us to use eU as a single parent with a well-defined decay rate for He and ZR dating. It also considers the change of the daughter-production rate over geological time instead of using present-time production rates. Härtel et al. (2023) showed that the formulation

$$eU = 1.05 [U] + 0.24 [Th] + 0.0012 [Sm] \qquad \text{(A2)}$$

gives accurate results for samples at 30<t<1000 Ma, ~~The effective uranium concentration (eU) summarizes the α-producing U, Th, and Sm concentrations to a common decay rate of U. The formulation of eU in Eq. (2) follows the equations in Härtel et al. (2021) and differs from other eU calculations, e.g. that of Shuster et al. (2006) or Cooperdock et al. (2019) in two regards: First, it recalculates the parent concentrations to the decay rate of ^{238}U instead of total U. This enables us to use eU as a single parent with a well-defined decay rate for He and ZR dating. Second, it takes into account the change of daughter production rate over geological time instead of using present-time production rates. Figure A1 shows how the normalization coefficients for each α-producing element change with respect to the age of a sample. The coefficients in Eq. (2) give accurate results for samples at ages <1000 Ma (Härtel et al., 2023),~~ but may be modified if the expected ages for a set of samples are consistently higher or constrained well-enough to calculate them more accurately.

The coefficients for eU are derived in Eq. (A3)-(A9~~6~~). The starting point is the α-production equation:

$$N(\alpha) = 8 \frac{N_A \left[{}^{238}U \right]}{M_{238}} \left(e^{\lambda_{238} t} - 1 \right) + 7 \frac{N_A \left[{}^{235}U \right]}{M_{235}} \left(e^{\lambda_{235} t} - 1 \right) + 6 \frac{N_A \left[{}^{232}Th \right]}{M_{232}} \left(e^{\lambda_{232} t} - 1 \right) + \frac{N_A \left[{}^{147}Sm \right]}{M_{147}} \left(e^{\lambda_{147} t} - 1 \right) \qquad \text{(A3}~~1~~\text{)}.$$

N(α) is the number of alpha decays, N_A is the Avogadro constant, 8,7,6 and 1 are the numbers of alpha particle produced by the respective decay series, M are the molar masses, λ the decay constants and the symbols in brackets the concentrations (in units of mass) of each contributing parent nuclide. The constants used in the calculations are summarized in Table A1. Rescaling all summands to the terms of ^{238}U gives:

$$N(\alpha) = 8 \frac{N_A}{M_{238}} \left(e^{\lambda_{238} t} - 1 \right) \left[\left(1 + \frac{7 M_{238} \left(e^{\lambda_{235} t} - 1 \right)}{8 M_{235} \left(e^{\lambda_{238} t} - 1 \right)} \frac{w_{235}}{w_{238}} \right) \left[{}^{238}U \right] + \left(\frac{6 M_{238} \left(e^{\lambda_{232} t} - 1 \right)}{8 M_{232} \left(e^{\lambda_{238} t} - 1 \right)} \right) \left[{}^{232}Th \right] + \left(\frac{M_{238} \left(e^{\lambda_{147} t} - 1 \right)}{8 M_{147} \left(e^{\lambda_{238} t} - 1 \right)} \right) \left[{}^{147}Sm \right] \right] \text{(A4)}.$$

This equation can be simplified by replacing the weighted actinide concentrations in the square brackets by eU:

$$N(\alpha) = 8 \frac{N_A}{M_{238}} \left(e^{\lambda_{238} t} - 1 \right) [eU] \quad \text{(A5)}.$$

This results in:

$$eU = \left[\left(1 + \frac{7 M_{238} \left(e^{\lambda_{235} t} - 1 \right)}{8 M_{235} \left(e^{\lambda_{238} t} - 1 \right)} \frac{w_{235}}{w_{238}} \right) [U] w_{238} + \left(\frac{6 M_{238} \left(e^{\lambda_{232} t} - 1 \right)}{8 M_{232} \left(e^{\lambda_{238} t} - 1 \right)} \right) [Th] + \left(\frac{M_{238} \left(e^{\lambda_{147} t} - 1 \right)}{8 M_{147} \left(e^{\lambda_{238} t} - 1 \right)} \right) [Sm] w_{147} \right] \quad \text{(A6)}.$$

w_{235}, w_{238} and w_{147} are the mass fractions of the ^{235}U, ^{238}U and ^{147}Sm isotopes and the terms in square brackets are element concentrations. Equations (A7)–(A9) define the coefficients in (A1) for each element:

$$k_U = w_{238} + \frac{7 M_{238} \left(e^{\lambda_{235} t} - 1 \right)}{8 M_{235} \left(e^{\lambda_{238} t} - 1 \right)} w_{235} \quad \text{(A7)},$$

$$k_{Th} = \frac{6 M_{238} \left(e^{\lambda_{232} t} - 1 \right)}{8 M_{232} \left(e^{\lambda_{238} t} - 1 \right)} \quad \text{(A8)},$$

$$k_{Sm} = \frac{M_{238} \left(e^{\lambda_{147} t} - 1 \right)}{8 M_{147} \left(e^{\lambda_{238} t} - 1 \right)} w_{147} \quad \text{(A9)}.$$

Figure A1 shows how the normalization coefficients for each α-producing element change with respect to the age of a sample.

(A2).

eU is given by the term in the square brackets. For the elemental concentrations of the parents, this results in:

——————— (A3).

w_{235}, w_{238} and w_{147} are the mass fractions of the ^{235}U, ^{238}U and ^{147}Sm isotopes and the terms in square brackets are element concentrations. Equations (A4)-(A6) define the coefficients for each element:

——————————————— (A4),

——————————————— (A5),

——————————————— (A6).

eU is then defined as:

——————————————— (A7),

and the production equation simplifies to:

——————————————— (A
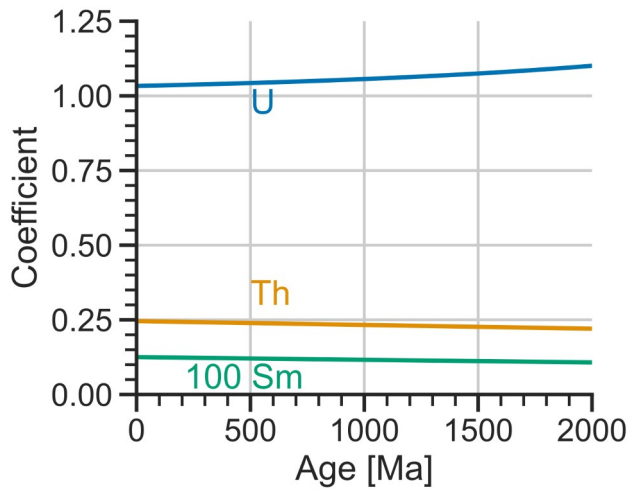
Fig. A1. Time-dependence of the coefficients for U, Th and
Sm (multiplied by 100) in the eU equation (2).

625

The time-dependence in Eq. (A4A7)-(A6A9) also allows iterative age calculation for He and ZR dating. This requires calculating eU from equation (A7A2) with a rough age estimate and then alternating between calculating the age from Eq. (1), and recalculating eU from Eq1. (A4A1) and (A7)-(A97) until the solutions converge.

630

Table A1. Coefficients and constants used in the calculations. The atomic masses and mass abundances are based on Holden et al. (2018), the decay constants are from Jaffey et al. (1971), Steiger and Jäger (1977), and Holden (1990). The decay constants are rounded to the first significant digit of their uncertainty.

Constant	Value
λ_{238}	$1.551\ 10^{-10}\ a^{-1}$
λ_{235}	$9.848\ 10^{-10}\ a^{-1}$
λ_{232}	$4.95\ 10^{-11}\ a^{-1}$
λ_{147}	$6.5\ 10^{-12}\ a^{-1}$
M_{238}	238.05 g/mol
M_{235}	235.04 g/mol
M_{232}	232.04 g/mol
M_{147}	146.91 g/mol
N_A	$6.022\ 10^{23}\ mol^{-1}$
w_{235}	0.0072
w_{238}	0.9928
w_{147}	0.1466

Appendix B: Units of daughter and parent concentrations

635   Daughter and parent concentrations can be expressed differently in external-detector-method FT and whole-grain He dating. Several criteria can be considered to find the right set of units for the D-P plot.

In He dating, the pairs of daughters (He) and parents (eU from U, Th, Sm) can either be expressed in units of abundance and mass (e.g., fmol and ng) or as concentrations (e.g., nmol/g and µg/g). The difference between these units is the normalization by the mass of the analyzed grain. For non-normalized data, the size or mass of the analyzed grains will introduce variation

640   into D and P that is unrelated to the age of the sample. In case the grains differ strongly in size, this may bias the pooled age towards the largest grains and the isochron age towards the smallest or the largest ones (see Appendix C). Rescaling the units of D and P to concentrations eliminates this potential bias. Furthermore, it is advantageous to correct the He concentration for α-ejection correction before calculating the age: correcting for α-ejection after age calculation introduces a positive bias to the age (e.g., Vermeesch, 2008). Therefore, the corrected He concentration should be used as daughter concentration for

645   plotting. In external-detector FT dating, a similar question of units arises concerning the use of either the spontaneous- and

induced-track counts or their track densities. In this case, it is advantageous to use the track densities instead of the counts to avoid bias towards big grains.

The specific units then determine the value of the constant c in Eq. (1). Re-arranging it to a daughter-production equation gives:

650 $$D = \frac{1}{c}\left(e^{\lambda t} - 1\right)[P] \tag{B1}.$$

For ZR dating, c results from equating Eq. (B1) and (A8):

$$c = \frac{M_{238}}{8 N_A} = 4.94\,10^{-23}\,g/a \tag{B2}.$$

Given input damage densities in 10^{16} α/g and eU concentrations in µg/g, c takes a value of 0.494 [10^{-16} µg/α].

For He dating, the same relationship as for ZR dating applies, with the difference of He concentrations usually being
655 reported in molar concentrations:

$$c = \frac{M_{238}}{8} = 29.76\,g/mol \tag{B3}.$$

If the input He concentrations are in in nmol/g and the eU concentrations in µg/g, c takes a value of 0.02976 [µg/nmol].

For FT dating, the constant c depends on measured experimental factors. This gives:

$$c = 0.5\,\lambda_D\,\zeta\,\rho_D \tag{B4}$$

660 for the external detector method, where 0.5 is the geometry factor, λ_D is the total decay constant for ^{238}U, ζ is the proportionality factor determined from dating an age reference material, and ρ_D the dosimeter track density (see Hurford, 2019). In this case, c is dimensionless because the spontaneous and induced-track counts densities are expressed in the same measurement units.

Laser-ablation FT dating requires a slightly different value for c because no dosimeter glass is involved in parent
665 measurement (see Vermeesch, 2019):

$$c = 0.5\,\lambda_D\,\zeta \tag{B5}.$$

In this case, the dimension of c depends on the units of parent measurement, e.g. as U concentration or as element ratio, e.g., U/Ca.

Appendix C: Age calculation and reporting

670 **C1 Mean ages**

For datasets showing a single age, it is attractive to report the arithmetic mean age due to its familiarity and simple calculation. However, the mean age is inadequate for summarizing most thermochronological ages. First, calculating a mean from ages determined by a logarithmic age equation as in (1) 'linearizes' the age equation and causes a negative bias compared to applying the logarithmic age equation to a mean D/P ratio. Second, even when directly applied to the ratio, the

675 arithmetic mean gives a biased age estimate, as can be shown from its relationship to the pooled age (see below; Pearson, 1896; Härtel et al., 2022a):

$$t_{mean} = t_{pooled}\left(1 - r_{DP}\, v_P\, v_D + v_P{}^2\right) \qquad\qquad \text{(C1).}$$

v_D and v_P are the variation coefficients (standard deviation divided by arithmetic mean) of the daughter and parent concentrations, and r_{DP} is their correlation coefficient. Equation (C1) shows that for the ideal proportional D-P relationship

680 ($r_{DP} = 1$, $v_D = v_P$), the mean and pooled ages are the same. In a less ideal case, the measurement error on the parent concentration increases v_P and – as it is independent of the daughter concentration – weaken the relationship between D and P (decreasing r_{DP}). This causes the mean age to increase with respect to the pooled age. It means that the mean age is biased towards higher ages under non-ideal daughter-parent relationships. This is especially problematic for the whole-grain He and laser-ablation FT methods, for which the analytical uncertainties are often too small to explain the observed age variation

685 (e.g., Fitzgerald et al., 2006; Ketcham et al., 2018). Essentially, measurement error on the parent concentration creates a right-skewed age distribution, whose mean increases with increasing variance and is biased towards higher ages.

A more robust alternative for calculating a central tendency is the pooled age, i.e., treating all analyzed grains as a single grain by summing up all daughter and parent concentrations. The age is then calculated by substituting the ratio of these sums for D/P in Eq. (1):

690
$$t_{pooled} = \frac{1}{\lambda}\ln\left(1 + c\,\frac{\sum D}{\sum P}\right) \qquad\qquad \text{(C2).}$$

Vermeesch (2008) pointed out that in the presence of outliers with high parent concentration or age, the pooled age is biased towards these grains. Also, Green (1981) and Galbraith and Laslett (1993) argued that the pooled age is not appropriate as sample age, if the age variation cannot be explained by the estimated uncertainties. However, in the case of clustered data (sect. 3.4~~3~~.2) or those forming a linear trend with zero intercept (sect. 3.4~~3~~.1) without outliers, the age variation is small so

695 that the bias on the pooled age can be assumed to be negligible. The uncertainty on the pooled age can be estimated from error propagation of the single-grain uncertainties. For He and ZR dating, this gives:

$$s\left(t_{pooled}\right) = t_{pooled}\sqrt{\frac{\sum s(D)^2}{\left(\sum D\right)^2} + \frac{\sum s(P)^2}{\left(\sum P\right)^2}} \qquad\qquad \text{(C3),}$$

with s representing the uncertainties on D, P, and t, respectively. FT dating requires to also take into account the uncertainty on c in Eq. (C2). For the EDM method, this gives (Galbraith, 2005):

$$s\left(t_{pooled}\right)=t_{pooled}\sqrt{\left(\frac{s(\zeta)}{(\zeta)}\right)^2+\frac{1}{\sum N_s}+\frac{1}{\sum N_i}+\frac{1}{\sum N_d}} \qquad \text{(C4)}.$$

N_s, N_i and N_d are the spontaneous, induced, and dosimeter track counts, respectively; ζ and $s(\zeta)$ are the calibration factor and its uncertainty.

For laser-ablation FT dating, the uncertainty on the pooled age is:

$$s\left(t_{pooled}\right)=t_{pooled}\sqrt{\left(\frac{s(\zeta)}{(\zeta)}\right)^2+\frac{1}{\sum N_s}+\frac{\sum s(P)^2}{\left(\sum P\right)^2}} \qquad \text{(C5)}.$$

If the ages from a dataset are over-dispersed due to the uncertainties not reflecting the variation in the data, it may be advantageous to estimate the uncertainty of the pooled age directly from the variation in D and P concentrations (e.g., Pearson, 1896):

$$s\left(t\right)=t\sqrt{\frac{v_D^2+v_P^2-r_{DP}v_D v_P}{n}} \qquad \text{(C6)}.$$

v_D and v_P represent the variation coefficients of D and P, and r_{DP} is the correlation coefficient for the D-P relationship. Equation (C6) may give a more realistic uncertainty estimate than those in Eq. (C3)-(C5) if the data are slightly over-dispersed. For strongly scattered data, however, (C6) gives a large uncertainty, confirming that a single sample age may be meaningless.

C2 Isochron ages

For systematically offset data (sect. 3.4̶3̶.3), the single-grain ages and the pooled age are offset in the same direction and give erroneously high or low ages (see sect. 2.3). In this case, it is advantageous to calculate an isochron age by fitting a regression line to the D-P data and replacing D/P in Eq. (1) by the slope m:

$$t_{isochron}=\frac{1}{\lambda}\ln\left(1+cm\right) \qquad \text{(C7)}.$$

The uncertainty on the isochron age results from propagation of the slope's uncertainty. This logarithmic age equation avoids the bias of the isochron age identified by Vermeesch (2008) for a linear age equation.

Typical algorithms for fitting isochrons are uncertainty-weighted (York, 1968; Kullerud, 1991) and robust regression (Huber, 1981; Powell et al., 2020). Both of these assign weights to each data point: the former based on the measured uncertainty, the latter based on the uncertainty and the distance of each point from a linear 'spine' in the data. Robust regression is therefore useful for datasets in which single grains fall off well-defined trends. However, its benefits are limited

in the case of many grains deviating from the trend. These regression algorithms, together with the classic least-squares regression are implemented in Incaplot.

In general, data at the low- and high-parent ends of the distribution and data with small uncertainties have a strong influence on the isochron age, making it sensitive for outliers. Its use should therefore be limited to cases of systematic offset in the D-P relationship. Apart from the isochron age, the intercept may also contain important information for the interpretation and should be reported together with the age (sect. 3.43.3).

The mean square weighted deviation (MSWD; or the spine width for robust isochrons) of the isochron provides information on how well the isochron fits the data. An MSWD within the confidence interval (Table C1) indicates that the variation of the data about the isochron is within the range expected from the input uncertainties. A high MSWD outside the confidence interval (Table C1) denotes over-dispersed data, whose variation is not explained by the input uncertainties alone – this may either point to unidentified sources of error or inter-grain variation of true ages within a sample. For He and laser-ablation FT data, whose sources of error are not yet well understood, these metrics have to be used with caution.

A standard practice to account for over-dispersed data in geochronology is to expand the uncertainty of the isochron age, multiplying it by $\sqrt{MSWD}$ (e.g., Ludwig, 2012).

Table C1. Confidence intervals (95 %) for the MSWD and the spine width for isochron fits (n-2 degrees of freedom). The MSWD intervals are based on Wendt and Carl (1991), the intervals for the spine width are from Powell et al. (2020).

	MSWD		Spine width	
n	Lower boundary	Upper boundary	Lower boundary	Upper boundary
10	0.50	2.00	0.31	1.55
15	0.61	1.78	0.4	1.5
30	0.73	1.53	0.58	1.39
60	0.81	1.37	0.71	1.28

C3 Age mixtures

Apart from the simple cases, discrete or continuous mixtures of ages may occur. There are two strategies to deal with discrete age components in a sample (sect. 3.43.5): mixture modeling (e.g., Galbraith and Laslett, 1993; Galbraith, 2005; Vermeesch, 2019), or splitting the data into different groups and calculating sample ages for each of them.

A continuous age mixture occurs if a sample contains grains with a wide range of kinetic properties responding differently to same thermal history (e.g., Vermeesch, 2019) – each grain then acts as single thermochronometer. An example could be the apatite FT age in a monotonously cooled plutonic rock with grains of different Cl/F ratio. In this case, the intra-sample age variation reflects both, the measurement error and the true-age variation between grains. This distribution is best described

by a 'random effects model' and the age to be reported is the central age (Galbraith and Laslett, 1993) – the dispersion parameter describes the variation in true ages. Note however, that it is necessary to relate the single-grain age to a kinetic parameter such as grain size, mineral chemistry, or measured radiation damage (Fig. ~~4a~~3e) to justify the use of a continuous mixture of ages. Galbraith (2005) and Vermeesch (2019) provide further discussion and calculation algorithms of the central age for FT dating, and Vermeesch (2008) for He dating. For complex data that cannot be described by a discrete or continuous mixture, we suggest to report the range of single-grain ages, which requires no additional assumptions.

Author contribution

BH: Conceptualization, Methodology, Formal analysis, Visualization Writing – original draft preparation; EE: Conceptualization, Visualization, Funding acquisition, Writing – review and editing.

Competing interests

The authors declare that they have no conflict of interest.

Acknowledgements and Funding

This research was funded by the ~~Natural Sciences and Engineering Research Council of Canada (NSERC) RGPIN-2018-03932 (Eva Enkelmann) and the~~ University of Calgary Eyes High postdoctoral match funding to Birk Härtel~~,~~ the Natural Sciences and Engineering Research Council of Canada (NSERC) RGPIN-2024-03863 (Eva Enkelmann) and the American Chemical Society – PRF # 67107-ND8 (Eva Enkelmann).

Code/Data availability

The synthetic D-P data shown in Fig. 1 are available as a supplementary file to this article. Incaplot is available as standalone executable for MacOS and Windows OS at https://zenodo.org/records/8233941.

References

Ault, A.K., Guenthner, W.R., Moser, A.C., Miller, G.H., and Refsnider, K.A.: Zircon grain selection reveals (de)coupled metamictization, radiation damage, and He diffusivity, Chem. Geol., 490, 1-12, https://doi.org/10.1016/j.chemgeo.2018.04.023, 2018.

Armstrong, E.M., Ault, A.K., Kaempfer, J.M., and Guenthner, W.R.: Connecting visual metamictization to radiation damage to expand applications of zircon (U-Th)/He thermochronometry, Chem. Geol., 121949, https://doi.org/10.1016/j.chemgeo.2024.121949, 2024.

Barbarand, J., Carter, A., Wood, I., and Hurford, T.: Compositional and structural control of fission-track annealing in apatite, Chem. Geol., 203, 107-137, https://doi.org/10.1016/S0009-2541(02)00424-2, 2003.

Baughman, J.S., and Flowers, R.M.: Deciphering a 2 Gyr-long thermal history from a multichronometer (U-Th)/He study of the Phalaborwa carbonatite, Kaapvaal craton, South Africa, Geochem., Geophys., Geosys, 19, 1581-1594, https://doi.org/10.1029/2017GC007198, 2018.

Baughman, J., Flowers, R.M., Metcalf, J.R. and Dhansay, T.: Influence of radiation damage on titanite He diffusion kinetics, Geochim. Cosmochim. Acta, 205, 50-64, https://doi.org/10.1016/j.gca.2017.01.049, 2017.

Carter, A.: Thermochronology on sand and sandstones for stratigraphic and provenance studies, in: Fission-track thermochronology and its application to Geology, edited by: Malusà, M.G., and Fitzgerald, P.G., Springer International Publishing, New York, pp. 259-268, https://doi.org/10.1007/978-3-319-89421-8_14, 2019.

Chayes, F.: On ratio correlation in petrography, J. Geol., 57, 239-254, 1949.

Cooperdock, E.H.G., Ketcham, R.A., and Stockli, D.F.: Resolving the effects of 2-D versus 3-D grain measurements on apatite (U-Th)/He age data and reproducibility, Geochronology, 1, 17-41, https://doi.org/10.5194/gchron-1-17-2019, 2019.

Deliens, M., Delhal, J., and Tarte, P.: Metamictization and U-Pb systematics – a study by infrared absorption spectrometry of Precambrian zircons, Earth Planet. Sci. Lett., 33, 331-344, https://doi.org/10.1016/0012-821X(77)90085-1, 1977.

Dunkl, I.: Trackkey: a Windows program for calculation and graphical presentation of fission track data, Comput. Geosci., https://doi.org/10.1016/S0098-3004(01)00024-3, 28. 3-12, 2002.

Fanale, F.P., and Kulp, J.L.: The helium method and the age of the Cornwall, Pennsylvania magnetite ore, Econ. Geol., 57, 735-746, https://doi.org/10.2113/gsecongeo.57.5.735, 1962.

Fitzgerald, P.G., Baldwin, S.L., Webb, L.E., and O'Sullivan, P.B.: Interpretation of (U-Th)/He single grain ages from slowly cooled crustal terranes: a case study from the Transantarctic Mountains of southern Victoria Land, Chem. Geol., 225, 91-120, https://doi.org/10.1016/j.chemgeo.2005.09.001, 2006.

Flowers, R.M., and Kelley, S.A.: Interpreting data dispersion and "inverted" dates in apatite (U-Th)/He and fission-track datasets: An example from the US midcontinent, Geochim. Cosmochim. Acta, 75, 5169-5186, https://doi.org/10.1016/j.gca.2011.06.016, 2011.

Flowers, R.M., Ketcham, R.A., Shuster, D.L., and Farley, K.A.: Apatite (U-Th)/He thermochronometry using a radiation damage accumulation and annealing model, Geochim. Cosmochim. Acta, 73, 2347-2365, https://doi.org/10.1016/j.gca.2009.01.015, 2009.

Flowers, R.M., Ketcham, R.A., Enkelmann, E., Gautheron, C., Reiners, P.W., Metcalf, J.R., Danišik, M., Stockli, D.F., and Brown, R.W.: (U-Th)/He chronology: Part 2. Considerations for evaluating, integrating, and interpreting conventional individual aliquot data, Geol. Soc. Am. Bull., 135, 137-161, https://doi.org/10.1130/B36268.1, 2022.

Galbraith R.F.: Statistics for fission track analysis, Chapman & Hall, Boca Raton, Florida, 219 pp., ISBN: 9780367392796, 2005.

Galbraith, R.F., and Laslett, G.M.: Statistical models for mixed fission track ages, Nucl. Tracks Radiat. Meas., 21, 459-470, https://doi.org/10.1016/1359-0189(93)90185-C, 1993.

Green, P.F.: A new look at statistics in fission-track dating, Nucl. Tracks, 55, 77-86, https://doi.org/10.1016/0191-278X(81)90029-9, 1981.

Green, P.F., Crowhurst, P.V., Duddy, I.R., Japsen, P., and Holford, S.P.: Conflicting (U-Th)/He and fission track ages in apatite: Enhanced He retention, not anomalous annealing behaviour, Earth Planet. Sci. Lett., 250, 407-427, https://doi.org/10.1016/j.epsl.2006.08.022, 2006.

Guenthner, W.R., Reiners, P.W., Ketcham, R.A., Nasdala, L., and Giester, G.: Helium diffusion in natural zircon: Radiation damage, anisotropy, and the interpretation of (U-Th)/He thermochronology, Am. J. Sci., 313, 145-198, https://doi.org/10.2475/03.2013.01, 2013.

Guenthner, W.R., Reiners, P.W., Hendriks, D., and Tilberg, M.: Zircon, titanite, and apatite (U-Th)/He ages and age-eU correlations from the Fennoscandian Shield, southern Sweden, Tectonics, 36, 1254-1274, https://doi.org/10.1002/2017TC004525, 2017.

Härtel, B.: Incaplot (v1.37), https://doi.org/10.5281/zenodo.8233941, 2024.

Härtel, B., Jonckheere, R., Wauschkuhn, B., Hofmann, M., Frölich, S., and Ratschbacher, L.: Zircon Raman dating: Age equation and calibration, Chem. Geol., 579, 120351, https://doi.org/10.1016/j.chemgeo.2021.120351, 2021

Härtel, B., Jonckheere, R., Krause, J., and Ratschbacher, L.: Spurious age-eU associations in thermochronology, Earth Planet. Sci. Lett., 117870, https://doi.org/10.1016/j.epsl.2022.117870, 2022a.

Härtel, B., Jonckheere, R., and Ratschbacher, L.: Multi-band Raman analysis of radiation damage in zircon for thermochronology: Partial annealing and mixed signals, Geochem. Geophys. Geosys., 23, e2021GC010182, https://doi.org/10.1029/2021GC010182, 2022b.

Härtel, B., Matthews, W.A., and Enkelmann, E.: Duluth Complex FC1 apatite and zircon: reference materials for (U-Th)/He dating? Geostand. Geoanal. Res., 47, 669-681, https://doi.org/10.1111/ggr.12492, 2023.

He, J., Thomson, S.N., Reiners, P.W., Hemming, S.R., and Licht, C.J.: Rapid erosion of the central Transantarctic Mountains at the Eocene-Oligocene transition: Evidence from skewed (U-Th)/He date distributions near Beardmore Glacier, Earth Planet. Sci. Lett., 567, 117009, https://doi.org/10.1016/j.epsl.2021.117009, 2021.

835 Heller, B.M., Lünsdorf, N.K., Dunkl, I., Molnár, F., and von Eynatten, H.: Estimation of radiation damage in titanites using Raman spectroscopy, Am. Min., 104, 857-868, https://doi.org/10.2138/am-2019-6681, 2019.

Holden, N.E.: Total half-lives for selected nuclides, Pure Appl. Chem., 62, 941-958, https://doi.org/10.1351/pac199062050941, 1990.

Holden, N.E., Coplen, T.B., Böhlke, J.K., Tarbox, L.V., Benefield, J., de Laeter, J.R., Mahaffy, P.G., O`Connor, G., Roth, 840 E., Tepper, D.H., Walczyk, T., Wieser, M.E., and Yoneda, S.: IUPAC periodic table of the elements and isotopes (IPTEI) for the education community, Pure Appl. Chem., 90, 1833-2092, https://doi.org/10.1515/pac-2015-0703, 2018.

Holland, H.D., and Gottfried, D.: The effect of nuclear radiation on the structure of zircon, Acta Crystallogr., 8, 291-300, https://doi.org/10.1107/S0365110X55000947, 1955.

Hourigan, J.K., Reiners, P.W., and Brandon, M.T.: U-Th zonation-dependent alpha-ejection in (U-Th)/He chronometry, 845 Geochim. Cosmochim. Acta, 69, 3349-3365, https://doi.org/10.1016/j.gca.2005.01.024, 2005.

Huber, P.J.: Robust Statistics, John Wiley and Sons, Inc., New York, 305 pp., https://doi.org/10.1002/9780470434697, 1981.

Hurford, A.J.: An historical perspective on fission-track thermochronology, in: Fission-track thermochronology and its application to Geology, edited by: Malusà, M.G., and Fitzgerald, P.G., Springer International Publishing, New York, pp. 3-24, https://doi.org/10.1007/978-3-319-89421-8_1, 2019.

850 Issler, D. R., Grist, A. M., and Stasiuk, L. D.: Post-Early Devonian thermal constraints on hydrocarbon source rock maturation in the Keele Tectonic Zone, Tulita area, NWT, Canada, from multi-kinetic apatite fission track thermochronology, vitrinite reflectance and shale compaction, Bull. Can. Pet. Geol., 53, 405–431, https://doi.org/10.2113/53.4.405, 2005.

Jaffey, A.H., Flynn, K.F., Glendenin, L.E., Bentley, W.C., and Essling, A.M.: Precision measurement of half-lives and 855 specific activities of 235U and 238U, Phys. Rev. C, 4, 1889-1906, https://doi.org/10.1103/PhysRevC.4.1889, 1971.

Kempe, U., Trullenque, G., Thomas, R., Sergeev, S., Presnyakov, S., Rodionov, N., and Himcinschi, C.: Substitution-induced internal strain and high disorder in weakly radiation damaged hydrothermal zircon from Mt. Malosa, Malawi, Eur. J. Min., 30, 659-679, https://doi.org/10.1127/ejm/2018/0030-2739, 2018.

Ketcham, R.A., van der Beek, P., Barbarand, J., Bernet, M., and Gautheron, C.: Reproducibility of Thermal History 860 Reconstruction from Apatite Fission-Track and (U-Th)/He Data, Geochem. Geophys. Geosys., 19, 2411–2436, https://doi.org/10.1029/2018GC007555, 2018.

Kohn, B.P., Ketcham, R.A., Vermeesch, P., Boone, S.C., Hasebe, N., Chew, D., Bernet, M., Chung, L., Danišik, M., Gleadow, A.J.W., and Sobel, E.R.: Interpreting and reporting fission-track chronological data, Geol. Soc. Am. Bull. (2024), https://doi.org/10.1130/B37245.1, 2024.

865 Kullerud, L.: On the calculation of isochrons, Chem. Geol., 87, 115-124, https://doi.org/10.1016/0168-9622(91)90045-X, 1991.

Kulp, J. L., Volchok, H. L., and Holland, H. D.: Age from metamict minerals, Am. Min., 37, 709-718, 1952.

Li, Y., and Vermeesch, P.: Short communication: Inverse isochron regression for Re-Os, K-Ca and other chronometers, Geochronology, 3, 415-420, https://doi.org/10.5194/gchron-3-415-2021, 2021.

870 Liu, J., Glasmacher, U.A., Lang, M., Trautmann, C., Voss, K.-O., Neumann, R., Wagner, G. A., and Miletich, R.: Raman spectroscopy of apatite irradiated with swift heavy ions with and without simultaneous exertion of high pressure, Appl. Phys. A, 91, 17-22, https://doi.org/10.1007/s00339-008-4402-9, 2008.

Ludwig, K.R.: Isoplot/Ex Version 3.75: A geochronological toolkit for Microsoft Excel, Special Publication, 4, Berkeley Geochronology Center, 1-75, 2012.

875 Malusà, M.G.: A guide for interpreting complex detrital age patterns in stratigraphic sequences, in: Fission-track thermochronology and its application to Geology, edited by: Malusà, M.G., and Fitzgerald, P.G., Springer International Publishing, New York, pp. 279-293, https://doi.org/10.1007/978-3-319-89421-8_16, 2019.

Malusà, M.G., and Fitzgerald, P.G.: Application of thermochronology to geologic problems: bedrock and detrital approaches, in: Fission-track thermochronology and its application to Geology, edited by: Malusà, M.G., and Fitzgerald, 880 P.G., Springer International Publishing, New York, pp. 191-209, https://doi.org/10.1007/978-3-319-89421-8_10, 2019.

Martin, P.E., Metcalf, J.R., and Flowers, R.M.: Calculation of uncertainty in the (U-Th)/He system, Geochronology, 5, 91-107, https://doi.org/10.5194/gchron-5-91-2023, 2023.

Miltich, L.: Low temperature cooling history of Archean gneisses and Paleoproterozic granites of southwestern Minnesota, B.A. thesis, Carleton College, Minnesota, 58 pp, 2005.

885 Murray, K.E., Orme, D.A., and Reiners, P.W.: Effects of U-Th-rich grain boundary phases on apatite helium ages, Chem. Geol., 390, 135-151, https://doi.org/10.1016/j.chemgeo.2014.09.023, 2014.

Nasdala, L., Irmer, G., and Wolf, D.: The degree of metamictization in zircon: A Raman spectroscopic study, Eur. J. Min., 7, 471-478, 1995.

Nasdala, L., Wenzel, M., Vavra, G., Irmer, G., and Kober, B.: Metamictisation of natural zircon: accumulation versus 890 thermal annealing of radioactivity-induced damage, Contrib. Min. Petrol., 141, 125-144, https://doi.org/10.1007/s004100000235, 2001.

Nicolaysen, L.O.: Graphic interpretation of discordant age measurements on metamorphic rocks, Ann. N. Y. Acad. Sci., 91, 198-206, https://doi.org/10.1111/j.1749-6632.1961.tb35452.x, 1961.

Orme, D.A., Reiners, P.W., Hourigan, J.K., and Carrapa, B.: Effects on inherited cores and magmatic overgrowths on zircon (U-Th)/He ages and age-eU trends from Greater Himalayan sequence rocks, Mount Everest region, Tibet, Geochem. Geophys. Geosys., 16, 2499-2507, https://doi.org/10.1002/2015GC005818, 2015.

Pearson, K.: Mathematical contribution to the theory of evolution. On a form of spurious correlation which may arise when indices are used in the measurement of organs, Proc. R. Soc. Lond., 60, 489-498, 1896.

Pickering, J., Matthews, W., Enkelmann, E., Guest, B., Sykes, C., and Koblinger, B.M.: Laser ablation (U-Th-Sm)/He dating of detrital apatite, Chem. Geol., 548, 119683, https://doi.org/10.1016/j.chemgeo.2020.119683, 2020.

Powell, R., Green, E.C.R., Marillo Sialer, E., and Woodhead, J.: Robust isochron calculation, Geochronology, 2, 325-342, https://doi.org/10.5194/gchron-2-325-2020, 2020.

Recanati, A., Gautheron, C., Barbarand, J., Missenard, Y., Pinna-Jamme, R., Tassan-Got, L., Carter, A., Douville, E., Bordier, L., Pagel, M., and Gallagher, K.: Helium trapping in apatite damage: Insights from (U-Th-Sm)/He dating of different granitoid lithologies, Chem. Geol., 470, 116-131, https://doi.org/10.1016/j.chemgeo.2017.09.002, 2017.

Ritter, W., and Märk, T.D.: Optical studies of radiation damage and its annealing in natural fluorapatite, Nucl. Instr. Meth. Phys. Res. B1, 394-397, https://doi.org/10.1016/0168-583X(84)90098-3, 1984.

Shuster, D.L., Flowers, R.M., and Farley, K.A.: The influence of natural radiation damage on helium diffusion kinetics in apatite, Earth. Planet. Sci. Lett., 249, 148-161, https://doi.org/10.1016/j.epsl.2006.07.028, 2006.

Steiger, R.H., and Jäger, E.: Subcommission on geochronology: convention on the use of decay constants in geo- and cosmochronology, Earth Planet. Sci. Lett., 36, 359-362, https://doi.org/10.1016/0012-821X(77)90060-7, 1977.

Stockli, D.F., Linn, J.K., Walker, J.D., and Dumitru, T.A.: Miocene unroofing of the Canyon Range during extension along the Sevier Desert Detachment, west central Utah, Tectonics, 20, 289-307, https://doi.org/10.1029/2000TC001237, 2001.

Sturrock, C.P., Flowers, R.M., and Macdonald, F.A.: The Late Great Unconformity of the Central Canadian Shield, Geochem. Geophys. Geosys., 22, e2020GC009567, https://doi.org/10.1029/2020GC009567, 2021.

Tripathy-Lang, A., Hodges, K.V., Monteleone, B.D., and van Soest, M.C.: Laser (U-Th)/He thermochronology of detrital zircons as a tool for studying surface processes in modern catchments, J. Geophys. Res.: Earth Surf., 118, 1333-1341, https://doi.org/10.1002/jgrf.20091, 2013.

Troch, J., Ellis, B.S, Schmitt, A.K., Bouvier, A.-S., and Bachmann, O.: The dark side of zircon: textural, age, oxygen isotopics and trace element evidence of fluid saturation in the subvolcanic reservoir of the Island Park-Mount Jackson Rhyolite, Yellowstone (USA), Contrib. Min. Petrol., 173, 54, https://doi.org/10.1007/s00410-018-1481-2, 2018.

Vermeesch, P.: Three new ways to calculate average (U-Th)/He ages, Chem. Geol., 249, 339-347, https://doi.org/10.1016/j.chemgeo.2008.01.027, 2008.

Vermeesch, P.: HelioPlot, and the treatment of overdispersed (U-Th-Sm)/He data, Chem. Geol., 271, 108-111,
925   https://doi.org/10.1016/j.chemgeo.2010.01.002, 2010.

Vermeesch, P.: Statistics for fission-track thermochronology, in: Fission-track thermochronology and its application to Geology, edited by: Malusà, M.G., and Fitzgerald, P.G., Springer International Publishing, New York, pp. 109-122, https://doi.org/10.1007/978-3-319-89421-8_6, 2019.

Vermeesch, P., and Tian, Y.: Thermal history modelling: HeFty vs. QTQt, Earth-Sci. Rev., 139, 279-290,
930   https://doi.org/10.1016/j.earscirev.2014.09.010, 2014.

Vermeesch, P., Seward, D., Latkoczy, C., Wipf, M, Günther, D., and Bauer, H.: α-emitting mineral inclusions in apatite, their effect on (U-Th)/He ages, and how to reduce it, Geochim. Cosmochim. Acta, 71, 1737-1746, https://doi.org/10.1016/j.gca.2006.09.020, 2007.

Wendt, I., and Carl, C.: The statistical distribution of the mean squared weighted deviation, Chem. Geol., 86, 275-285,
935   https://doi.org/10.1016/0168-9622(91)90010-T, 1991.

Wernicke, R.S., and Lippolt, H.J.: Botryoidal hematite from the Schwarzwald (Germany): heterogeneous uranium distributions and their bearing on the helium dating method, Earth Planet. Sci. Lett., 114, 287-300, https://doi.org/10.1016/0012-821X(93)90031-4, 1993.

Willett, C.D, Fox, M., and Shuster, D.L.: A helium-based model for the effects of radiation damage annealing on helium
940   diffusion kinetics in apatite, Earth Planet. Sci. Lett., 477, 195-204, https://doi.org/10.1016/j.epsl.2017.07.047, 2017.

Wolfe, M.R., and Stockli, D.F.: Zircon (U-Th)/He thermochronometry in the KTB drill hole, Germany, and its implications for bulk He diffusion kinetics in zircon, Earth Planet. Sci. Lett., 295, 69-82, https://doi.org/10.1016/j.epsl.2010.03.025, 2010.

York, D.: Least squares fitting of a straight line with correlated errors, Earth Planet. Sci. Lett., 5, 320–324, https://doi.org/10.1016/S0012-821X(68)80059-7, 1968.

945   Zeigler, S.D., Metcalf, J.R., and Flowers, R.M.: A practical method for assigning uncertainty and improving the accuracy of alpha-ejection corrections and eU concentrations in apatite (U–Th) / He chronology, Geochronology, 5, 197-228, https://doi.org/10.5194/gchron-5-197-2023, 2023.